Dynamic Harris current sheet thickness from Cluster current density and plasma measurements

S. M. Thompson, M. G. Kivelson, K. K. Khurana, R. L. Mcpherron, J. M. Weygand, A. Balogh, H. Rème, L. M. Kistler

Dynamic Harris current sheet thickness from Cluster current density and plasma measurements

S. M. Thompson,[1,2] M. G. Kivelson,[1,2] K. K. Khurana,[1,2] R. L. McPherron,[1,2] J. M. Weygand,[1] A. Balogh,[3] H. Réme,[4] and L. M. Kistler[5]

Received 30 July 2004; revised 22 November 2004; accepted 17 December 2004; published 19 February 2005.

[1] We use the first accurate measurements of current densities in the plasma sheet to calculate the half-thickness and position of the current sheet as a function of time. Our technique assumes a Harris current sheet model, which is parameterized by lobe magnetic field B_0, current sheet half-thickness h, and current sheet position z_0. Cluster measurements of magnetic field, current density, and plasma pressure are used to infer the three parameters as a function of time. We find that most long timescale (6–12 hours) current sheet crossings observed by Cluster cannot be described by a static Harris current sheet with a single set of parameters B_0, h, and z_0. Noting the presence of high-frequency fluctuations that appear to be superimposed on lower frequency variations, we average over running 6-min intervals and use the smoothed data to infer the parameters $h(t)$ and $z_0(t)$, constrained by the pressure balance lobe magnetic field $B_0(t)$. Whereas this approach has been used in previous studies, the spatial gradients now provided by the Cluster magnetometers were unavailable or not well constrained in earlier studies. We place the calculated half-thicknesses in a magnetospheric context by examining the change in thickness with substorm phase for three case study events and 21 events in a superposed epoch analysis. We find that the inferred half-thickness in many cases reflects the nominal changes experienced by the plasma sheet during substorms (i.e., thinning during growth phase, thickening following substorm onset). We conclude with an analysis of the relative contribution of $\partial B_Z/\partial X$ to the cross-tail current density during substorms. We find that $\partial B_Z/\partial X$ can contribute a significant portion of the cross-tail current around substorm onset.

Citation: Thompson, S. M., M. G. Kivelson, K. K. Khurana, R. L. McPherron, J. M. Weygand, A. Balogh, H. Réme, and L. M. Kistler (2005), Dynamic Harris current sheet thickness from Cluster current density and plasma measurements, *J. Geophys. Res.*, *110*, A02212, doi:10.1029/2004JA010714.

1. Introduction

[2] The magnetotail, a fundamental reservoir of energy in the terrestrial magnetosphere, contains two bundles of magnetic flux that emerge from the poles and are swept antisunward on the nightside of the Earth, forming the magnetotail lobes. The magnetic field is directed primarily antisunward in the southern lobe and sunward in the northern lobe, the reversal requiring currents to flow from dawn to dusk across the magnetotail. *Ness* [1965] first observed the magnetotail current sheet with IMP 1. The current sheet itself is embedded in a plasma sheet of larger north-south extent that contains plasma from both the solar wind and the ionosphere. In the central plasma sheet, the thin surface across which the magnetic field reverses sign is called the neutral sheet.

[3] The primary mechanism by which energy is transferred to the magnetotail is reconnection between the interplanetary magnetic field and the closed magnetic field lines of the dayside magnetosphere. Energy transferred from the solar wind to the magnetosphere is stored in the magnetotail until instability triggers a reconfiguration of the tail to a lower energy state. The primary mechanism by which this reconfiguration occurs is generally thought to be magnetic reconnection that occurs during substorms. Tools for monitoring the structure and dynamics of the magnetotail current sheet can contribute usefully to improved descriptions of substorm phenomenology and the stability of the magnetotail.

[4] The geometry of the current sheet and its dependence on dipole tilt has been represented in increasingly sophisticated forms. The earliest models described a current sheet that bisected the magnetotail with a displaced circle [*Russell and Brody*, 1967], ellipse [*Fairfield*, 1980], or multiple

[1]Institute of Geophysics and Planetary Physics, University of California, Los Angeles, California, USA.
[2]Also at Department of Earth and Space Sciences, University of California, Los Angeles, California, USA.
[3]Department of Physics, Imperial College of Science, Technology and Medicine, London, UK.
[4]Centre d'Etude Spatiale des Rayonnements/Centre National de Recherche Scientifique, Toulouse, France.
[5]Space Science Center, Science and Engineering Research Center, University of New Hampshire, Durham, New Hampshire, USA.

0148-0227/05/2004JA010714

intersecting ellipses [*Dandouras*, 1988]. More recent models were based on the Dandouras model but incorporated dependences on dipole tilt, solar wind dynamic pressure, local time, and radial distance [e.g., *Hammond et al.*, 1994; *Li and Xu*, 2000]. These studies generally optimized a particular model for different spacecraft datasets by identifying locations of current sheet crossings and setting the parameters of the model by minimizing differences between the model and the observed locations. Overall, these models provide excellent predictions of the location and shape of the current sheet. Establishing the current density and thickness of the magnetotail current sheet and describing the temporal evolution of these parameters is a more difficult task.

[5] The simplest description of the magnetotail magnetic field and current density north-south profile is the one-dimensional Harris current sheet [*Harris*, 1962]:

$$B_x = B_0 \tanh\left(\frac{Z - z_0}{h}\right) \quad (1)$$

$$J_Y = \frac{B_0}{\mu_0 h}\,\mathrm{sech}^2\left(\frac{Z - z_0}{h}\right), \quad (2)$$

where B_0 is the lobe magnetic field, z_0 is the position of the current sheet, h is the current sheet half-thickness, B_X is the locally measured magnetic field, J_Y is the local current density, X is positive toward the Sun, Y is positive toward dusk, and Z is the local position of the observation point (i.e., spacecraft location), positive northward. The Harris current sheet model is an equilibrium solution of the Maxwell-Vlasov equations assuming Maxwellian particle distributions in a coordinate system with equal but opposite ion and electron flow velocities. Before the launch of Cluster, only single or rare multiple spacecraft observations of the current sheet were available. Single spacecraft observations could sometimes be fit to the magnetic profile of a Harris current sheet. The parameters of that fit could then be used to infer the current density. More accurate determination of the current density has remained elusive because single spacecraft provide no information about the instantaneous spatial gradient of the magnetic field. This problem was partially alleviated in 1978 and 1979 when ISEE 1 and 2 were located in similar orbits in the magnetotail.

[6] *McComas et al.* [1986], using ISEE 1 and 2 magnetometer data, calculated upper bounds of current sheet thickness and current density by examining three rapid crossings of the current sheet at $\sim$18 R_E downtail. The spacecraft were separated by $\sim$1 R_E in X_{GSM} and $\sim$0.5 R_E in Z_{GSM}. Differences of the magnetic field between the two spacecraft in a boundary normal coordinate system were used to infer current densities. The analysis revealed that the quiet current sheet is several ion gyroradii thick (typical ρ_i in the current sheet is $\sim$3000 km for a 5 keV ion in a 2 nT magnetic field) with a clear current density peak that is sometimes embedded in a plasma region several times thicker with lower current densities. *McPherron et al.* [1987] and *Sanny et al.* [1994] examined a current sheet crossing of ISEE 1 and 2 at a downtail distance of $\sim$13 R_E. The spacecraft were separated by $\sim$2 R_E in X_{GSM} but only a fraction of an R_E in Z_{GSM}. The spatial gradient of B_X with Z_{GSM} ($\Delta B_X/\Delta Z$) between the two spacecraft was used to infer current densities. These current densities were used to characterize a time-varying Harris current sheet in order to determine the thickness of the current sheet in the hour prior to a substorm onset. *Sanny et al.* [1994] found an average thickness of $\sim$5 R_E 1 hour before the substorm onset that decreased to less than 1 R_E just prior to onset. *Zhou et al.* [1997] also calculated current sheet thickness with current densities inferred from an ISEE 1 and 2 joint current sheet crossing at a downtail distance of $\sim$17 R_E. The two spacecraft were separated by $\sim$1 R_E in X_{GSM} and $\sim$0.5 R_E in Z_{GSM}. That study found that the current sheet thinned from $\sim$3 R_E to $\sim$1 R_E over $\sim$30 min following a southward turning of the interplanetary magnetic field. The authors linked the thinning to the growth phase of a substorm. Uncertainties remained in these ISEE studies because two-point spatial measurements of the magnetic field may not accurately represent the cross-tail current density and only a few events were analyzed. More recently, current densities have been directly calculated from Geotail ion and electron velocity moments [e.g., *Asano et al.*, 2004]. However, uncertainties in the velocities can compromise current densities calculated in this manner.

[7] Four point Cluster measurements enable us to infer vector current densities from the curl of the magnetic field ($\nabla \times \mathbf{B}$). Launched in 2000, the Cluster spacecraft are in inertially fixed eccentric polar orbits with apogee 19.6 R_E and perigee 4 R_E. The orbit apogee sweeps through the magnetotail between July and October of each year. Typical spacecraft separations were $\sim$1000 km in 2001, $\sim$3000 km in 2002, and $\sim$150 km in 2003. When the four spacecraft are in an optimum tetrahedral configuration, the nine spatial gradients of the magnetic field establish the curl and divergence of B in the limit of linear variations. In this study, current densities were evaluated using the technique of *Khurana et al.* [1996]. This technique assumes linear magnetic field variation between the spacecraft such that the tetrahedron centroid magnetic field can be expressed as a Taylor series.

[8] Several recent studies have addressed the structure of the current sheet using Cluster data. *Weygand et al.* [2005] often find turbulence present in the current sheet during elevated geomagnetic activity. Several case studies suggest that the cross-tail current sheet sometimes "bifurcates" or splits into two distinct sheets of current separated by a weaker current region [*Nakamura et al.*, 2002; *Runov et al.*, 2003; *Sergeev et al.*, 2003]. *Shen et al.* [2003] developed a technique for inferring the thickness of the current sheet based on the local radius of curvature of the magnetic field. This technique does not rely explicitly on current densities but does require knowledge of the local magnetic field gradient. This study found substorm growth phase thicknesses of less than 0.1 R_E for a case study event.

[9] Despite the likelihood that the current sheet is turbulent and that it may intermittently develop bifurcated or other more complex structure, many plasma sheet crossings appear to retain an underlying averaged structure that can be interpreted by representing it as a Harris current sheet whose parameters (thickness and center location) vary in time. In this study we have used the variation of the dominant

component of the magnetic field and the measured current densities during Cluster plasma sheet crossings to infer time-varying current sheet thickness and position assuming the structure of a Harris current sheet. In doing so, we have sought to determine if the Harris current sheet provides a meaningful average description of current sheet dynamics in the middle magnetotail.

2. Cluster Plasma Sheet Observations

[10] Figure 1 shows an example of a typical plasma sheet crossing observed with Cluster 4 Fluxgate Magnetometer (FGM) [*Balogh et al.*, 2001] and Cluster Ion Spectrometry Composition Distribution Function (CIS/CODIF) [*Rème et al.*, 2001] from 0900 to 1930 UT on 12 September 2001 in GSM coordinates. Cluster was located at (−18.5, 3, 1) R_E GSM. The panels from top to bottom are B_X, B_Y, B_Z, B, proton number density n (cm^{-3}), and proton temperature T (keV). The magnetometer data are 4-s spin-averages while CIS/CODIF data are 8-s resolution. The B_X component clearly shows the expected trend in the magnetic field as the spacecraft passes from the northern lobe (positive B_X), through the current sheet (minimum B), and into the southern lobe (negative B_X) over a period of approximately 9 hours. Two brief exits from the plasma sheet into the lobe occurred just after 1500 UT, as indicated by the decrease in proton density to near zero. There were two small substorms, identified in the auroral activity index *AE*, at ∼1320 UT and ∼1515 UT. The substorms are observed in the Cluster data as modest increases in B_Z (dipolarizations) and high-frequency fluctuations in all components of the magnetic field. The proton number densities and temperatures range from low values typical of the lobes ($n < 0.1$ cm^{-3}, $T \sim 100$ eV) to high values typical of the plasma sheet ($n \sim 0.5$ cm^{-3}, $T \sim 5$ keV).

[11] Figure 2 shows the inferred vector current density in GSM coordinates for the plasma sheet crossing of Figure 1. The four spacecraft average magnetic field B_X is shown in the top panel for reference. J_Y (Figure 2c) is largest and B_X is close to zero between 1200 and 1500 UT, as for a Harris-type current sheet. However, there are instances when J_X and J_Z are comparable to J_Y in magnitude (e.g., 1510 UT). The fluctuations in all three components of the current density are sometimes greater than the means and at times J_Y becomes negative (e.g., 1530 UT). The divergence of the magnetic field in current density units ($\nabla \times \mathbf{B}/\mu_0$, Figure 2f) provides an indication of the reliability of the inferred current densities. We arbitrarily treat as suspect intervals with $\nabla \times \mathbf{B}/\mu_0 > 0.5|\mathbf{J}|$. At such times the technique for inferring current densities is probably unreliable (i.e., the assumption of linear magnetic field variation between the spacecraft is invalid).

[12] The time series of B_X clearly shows that the current sheet is changing, possibly through motion or compression during the lengthy spacecraft traversal of the plasma sheet. Small-scale structure is pervasive, making it difficult to determine whether or not on some larger scale a Harris-type current sheet is present. The question we wish to address here is whether or not time averages of the magnetic field and current densities approximate a Harris-type current sheet. We will first examine whether it is ever reasonable to fit Cluster current sheet crossings with a static Harris current sheet model.

3. Static Harris Current Sheet Fits

[13] The long duration of a typical plasma sheet crossing in the Cluster data (6 to 12 hours for crossing purely through orbital motion) makes it improbable a priori that a static Harris current sheet model will be valid. Solar wind changes and geomagnetic activity including multiple substorms, flapping, and other dynamics will conspire to confuse the time series profile of the current sheet. As a result, a typical 6–12 hour time series may not appear Harris-like. However, the current sheet may still be Harris-like despite the complex time series. Cluster traversed a relatively quiescent current sheet on a few occasions in 2001 and 2002. An example of such a current sheet crossing on 22 September 2001 is shown in Figure 3 where we have plotted the four spacecraft mean B_X (i.e., the average of the B_X component measured by each of the four Cluster spacecraft) versus Z_{GSM} and the inferred current density J_Y versus Z_{GSM} for the time interval 0100–0900 UT. The Gauss-Newton method [*Dennis*, 1977] was used to obtain a nonlinear least-squares fit of equation (1) to the magnetic field B_X. The parameters (B_0, z_0, and h) were then used in equation (2) for the current density J_Y (gray traces). In addition, J_Y was fit independently of B_X (black dashed traces). The fit parameters are indicated at the top of the figure with an error of ±2 standard deviations (95% confidence interval). The 95% confidence interval is ∼1–3% of the parameter value itself, indicating a robust solution. The root mean square (RMS) error for each fit is 4.45 nT for the magnetic field B_X and 0.9 nA m^{-2} for the current density J_Y. The best fit half-thickness and position are nearly identical for both fits based on the magnetic field or the current density with values of $h \sim 0.4$ R_E and $z_0 \sim -1.7$ R_E, respectively. As a result, we can compare the RMS errors of the two independent fits by converting the current density RMS error to magnetic field units as $J_{RMS} h \mu_0 = (0.9\text{ nA m}^{-2})(0.4\text{ R}_E)(4\pi \times 10^{-7}\text{ Hm}^{-1}) = 2.9$ nT. We therefore conclude that the least-squares fits to the magnetic field (RMS error = 4.45 nT) and current density (RMS error = 2.9 nT) are comparable. However, the best fit lobe magnetic field B_0 differs significantly between the two fits (∼26 nT for the magnetic field and ∼17 nT for the current density). The parameters for the B_X fit reproduce the peak of J_Y but not the width of the profile whereas the independent fit to J_Y reproduces the width but not the peak.

[14] Of the 67 current sheet crossings we have identified in 2001, 2002, and 2003, approximately 10% can be reasonably well fit on the 6–12 hour timescale. This is because a time-stationary model of magnetic field and current density is rarely useful. A time-varying current sheet thickness and position are necessary to provide a better description of the dynamics observed during a Cluster current sheet crossing.

4. Time-Varying Harris Current Sheet Model Fit

[15] With knowledge of the magnetic field and of the vector current densities, one can establish the parameters of a time-varying Harris current sheet model. Equations (1)

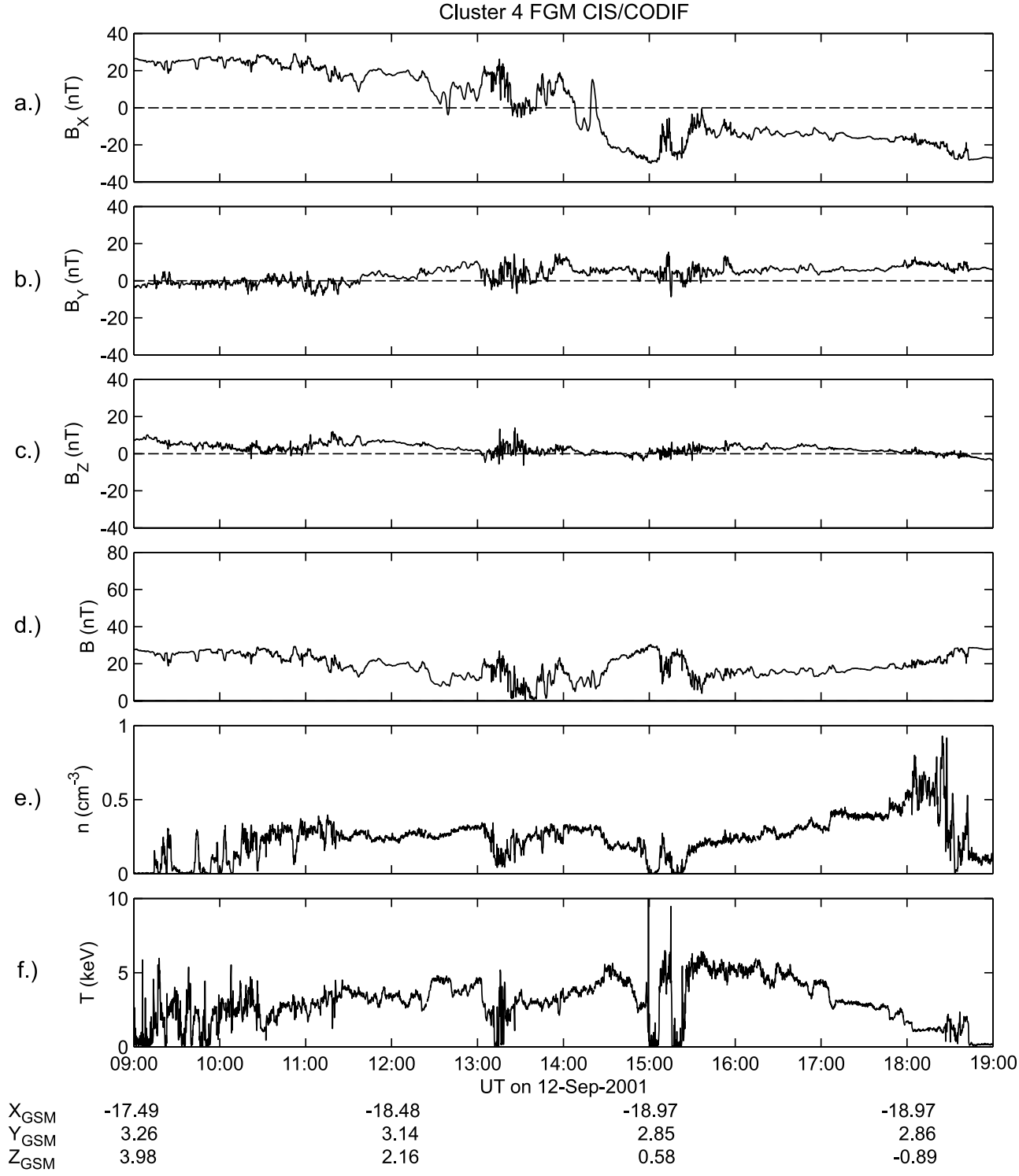

Figure 1. Cluster 4 Fluxgate Magnetometer (FGM) and Cluster Ion Spectrometry Composition Distribution Function (CIS/CODIF) observations for a plasma sheet crossing on 12 September 2001, 0900–1900 UT. Magnetometer data are in GSM coordinates. The GSM position of the Cluster tetrahedron is indicated along the bottom of the figure. (a) B_X, (b) B_Y, (c) B_Z, (d) B, (e) proton number density n, (f) proton temperature T.

and (2) establish the current sheet half-thickness $h(t)$ and its position $z_0(t)$ as functions of the lobe magnetic field $B_0(t)$:

$$\mathrm{h(t)} = \frac{\mathrm{B_0^2(t) - B_x^2(t)}}{\mu_0 \mathrm{B_0(t) J_y(t)}} \tag{3}$$

$$\mathrm{z_0(t)} = \mathrm{Z(t)} - \mathrm{h(t)} \tanh^{-1}\left(\frac{\mathrm{B_x(t)}}{\mathrm{B_0(t)}}\right). \tag{4}$$

This formalism was introduced by *Lui* [1993] as a means of describing the global behavior of the current sheet

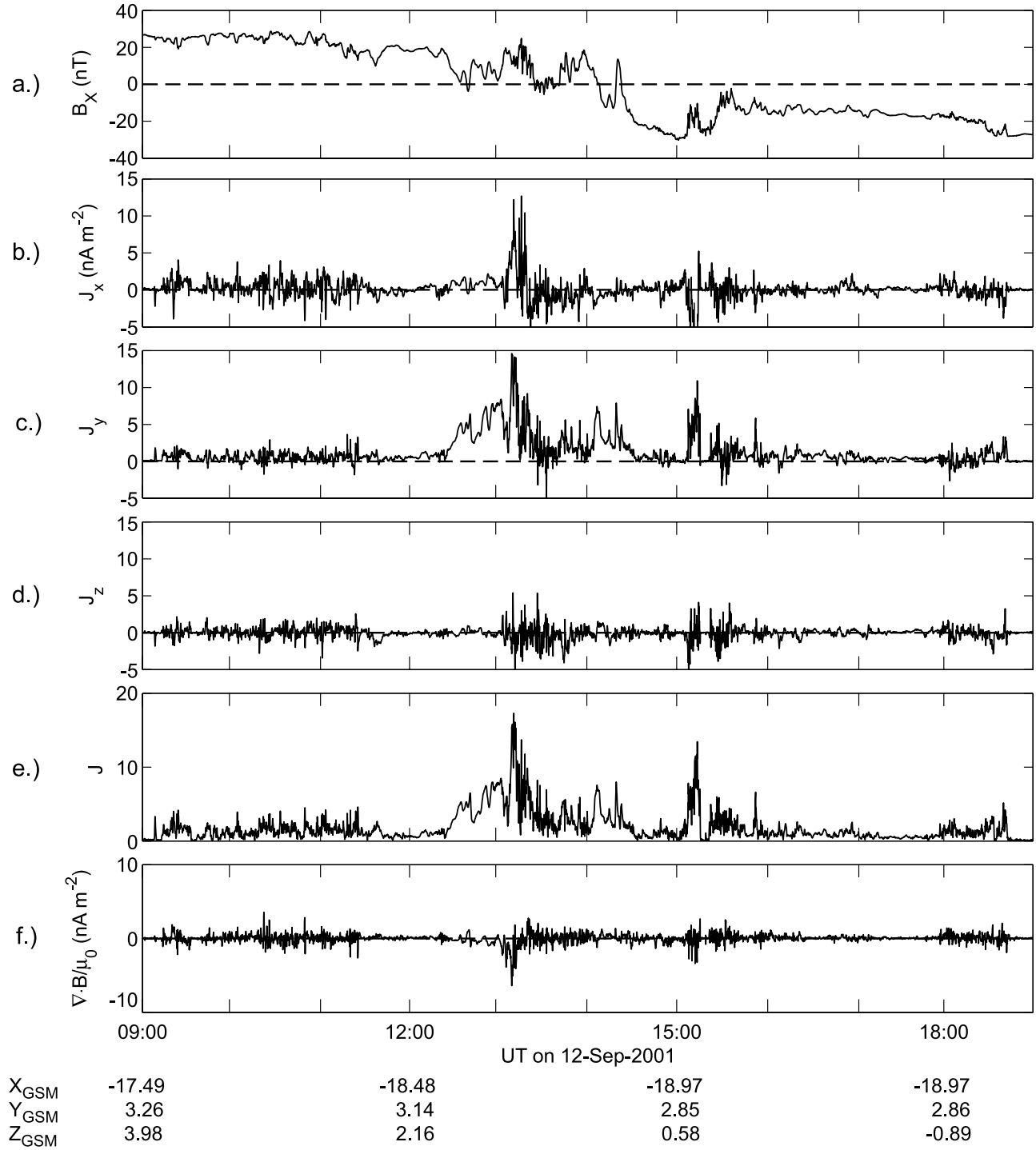

Figure 2. Inferred current densities for the plasma sheet crossing of 12 September 2001, 0900–1900 UT. (a) Four spacecraft average B_X, (b) J_X, (c) J_Y, (d) J_Z, (e) J, (f) $\nabla \times \mathbf{B}/\mu_0$.

using local measurements in or near the plasma sheet. *Sanny et al.* [1994] and *Zhou et al.* [1997] applied this concept using $\Delta B_X/\Delta Z$ to estimate cross-tail current density J_Y and ignoring the contribution of $\Delta B_Z/\Delta X$. Cluster determines J_Y more accurately than the approximate form, but in most cases the values differ little. Although $B_X(t)$, $J_Y(t)$, and $Z(t)$ are known, the time-varying lobe field $B_0(t)$ cannot be inferred from magnetometer measurements alone. In order to determine the time-varying lobe magnetic field, we make use of Cluster measurements of both $B(t)$ and plasma pressure and assume pressure balance of the sum of thermal and magnetic pressures across the magnetotail [*Rich et al.*, 1972]. The validity of this approximation in the magnetotail has been established by numerous studies [e.g., *Fairfield et al.*, 1981; *Baumjohann et al.*, 1990; *Matsumoto et al.*, 2001]. By equating the sum of the perpendicular proton thermal pressure and the magnetic

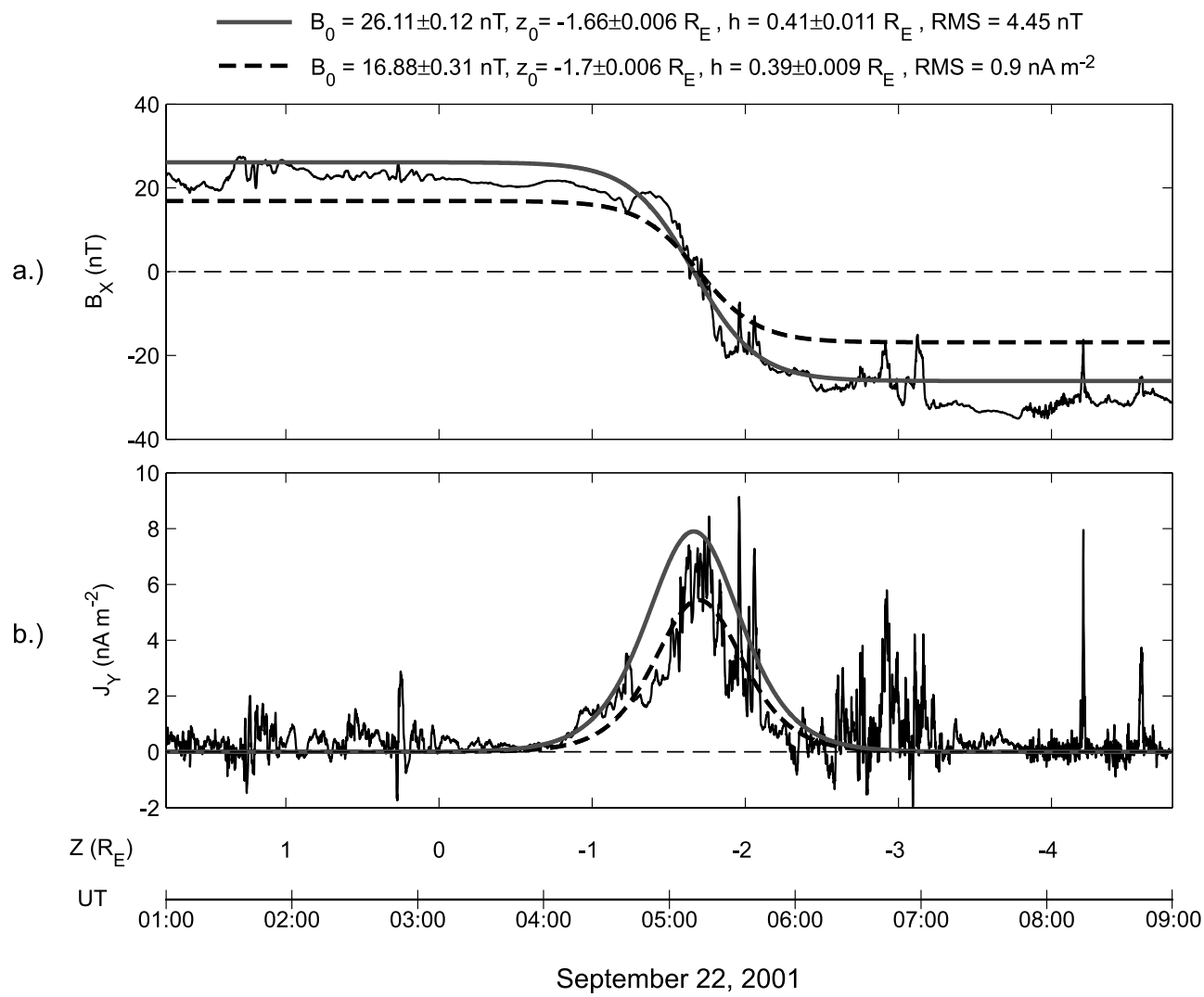

Figure 3. Nonlinear least-squares fit of a static Harris current sheet to a Cluster plasma sheet crossing on 22 September 2001 versus Z_{GSM} and UT. The gray traces indicate the fit for B_X independent of J_Y, while the dashed traces indicate the fit to J_Y independent of B_X. The 95% confidence level is indicated for each parameter at the top of the figure, as is the root-mean-square (RMS) error for each fit. (a) B_X, (b) J_Y.

pressure in the plasma sheet ($B(t)^2/2\mu_0 + p_\perp(t)$) to the magnetic pressure in the lobe ($B_0(t)^2/2\mu_0$), we find

$$B_0(t) = \sqrt{2\mu_0 p_\perp(t) + B(t)^2}, \quad (5)$$

where $p_\perp(t)$ is the thermal proton pressure perpendicular to the magnetic field and $B(t)$ is the locally measured magnetic field magnitude at time t. The Cluster CIS/CODIF perpendicular proton thermal pressure was calculated from diagonalization of the pressure tensor. We have added an additional 20% of $p_\perp$ to account for the electron and hot ion contribution to the thermal pressure [*Baumjohann*, 1993; *Matsumoto et al.*, 2001]. An example of a thermal and magnetic pressure profile in the plasma sheet on 22 September 2001, 0000–1000 UT is shown in Figure 4. The magnetometer data are four spacecraft averages while the CIS/CODIF data are from Cluster 1. The current sheet crossing can be identified as the time of peak thermal pressure and minimum magnetic pressure at ~0500 UT. The total pressure varies considerably between 0000 and 1000 UT. It is plausible to suggest that the variation reflects real changes in the magnetotail that occur over the extended interval of a Cluster plasma sheet crossing and calls for a time-varying model of the current sheet.

[16] Before providing quantitative results for current sheet parameters, we note further operational steps we have taken in applying equations (3) and (4). First, we resample the 4-s spin-averaged magnetic field and current density data at the 8-s resolution of the particle data and use equation (5) to obtain $B_0(t)$. Then, we take 6-min running averages shifted by one time step (8 s) of $B_0(t)$, $J_Y(t)$, and $B_X(t)$ in order to remove high-frequency fluctuations in the fields and currents so that we can focus on the relatively large-scale structure of the current sheet. The form of equation (3) makes it clear that the thickness and position parameters are useful only when J_Y is not extremely small. As J_Y approaches zero, $h(t)$ becomes infinite. In particular, current densities are small when Cluster is in the lobes.

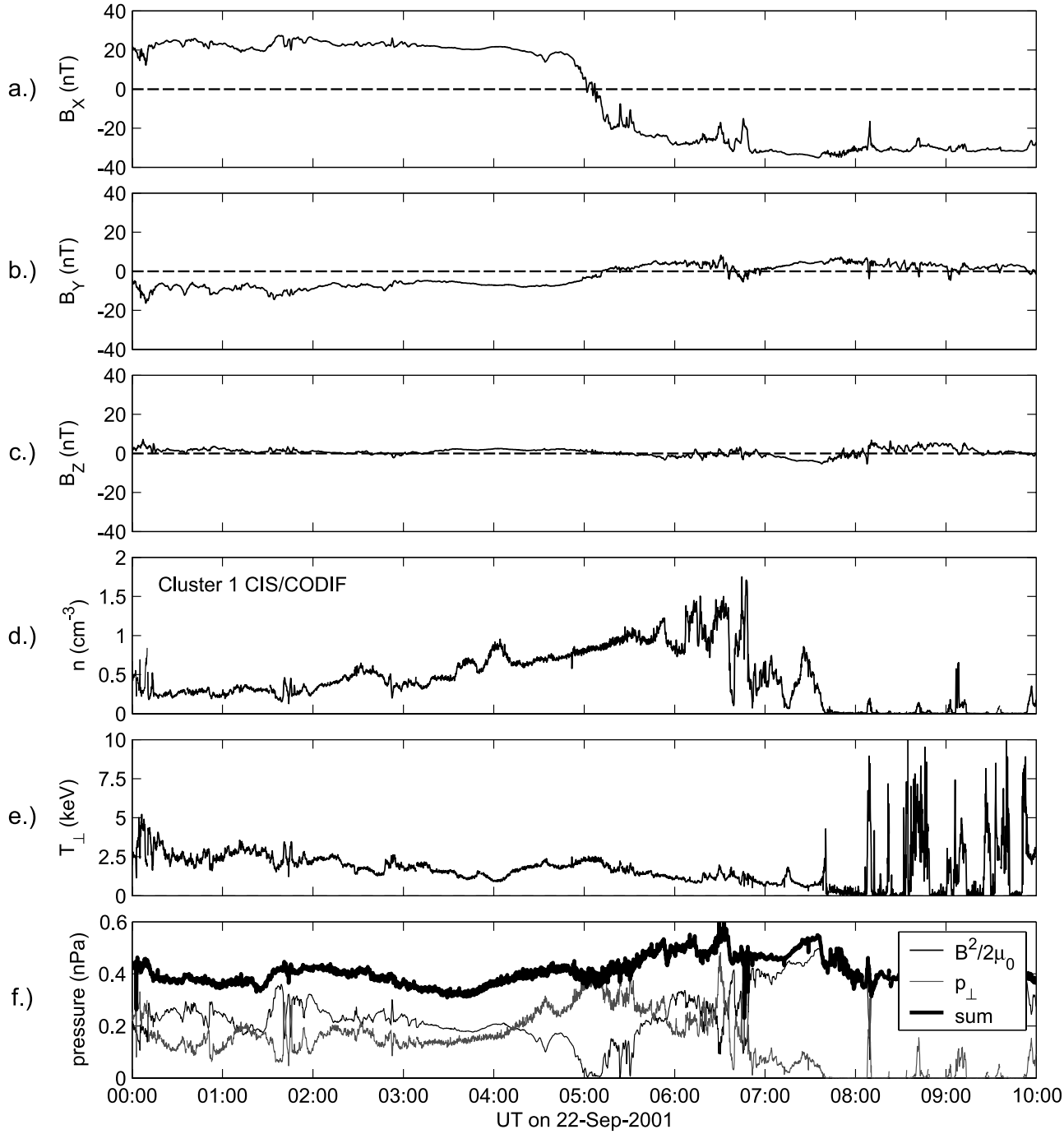

Figure 4. Pressure balance profile for a plasma sheet crossing on 22 September 2001, 0000–1000 UT. (a) Four spacecraft average B_X, (b) B_Y, (c) B_Z, (d) Cluster 1 CIS/CODIF proton number density n, (e) Cluster 1 CIS/CODIF proton temperature $T_\perp$, (f) magnetic (black trace), $p_\perp$ (gray trace), and total pressure (thick black trace).

However, small J_Y may be found even in the plasma sheet. Figure 2 shows that errors in the currents (thought to be of order $\nabla \times \mathbf{B}/\mu_0$) imply that very small values of J_Y are unreliable. Therefore points where $|J_Y| < 0.3$ nA m^{-2} have been removed from the 6-min running average J_Y, and this serves to eliminate infinities in $h(t)$. Finally, even though the average J_Y is predominantly positive, there are instances when it becomes negative. The negative currents are usually small and they have been ignored in our analysis. Using the dynamic Harris model fit, we next discuss how the current sheet behaves during three substorms.

5. Substorm Events

[17] We have studied three substorms, two in 2001 and another in 2002, during which Cluster was well placed to observe changes in the plasma sheet just inside of 20 R_E downtail. The positions of the Cluster tetrahedron in the X-

Y GSM plane at the times of the three substorm onsets are shown in Figure 5a, as are the X-Z GSM locations of the four spacecraft for the three substorm events (Figure 5b, 5c, and 5d).

5.1. The 13 September 2002 Event

[18] On 13 September 2002 Cluster was located at (−17.3, 2.17, 2.8) GSM at 1800 UT. In 2002 the Cluster spacecraft separation was ∼5000 km. Figure 6 shows the solar wind observations at ACE from 1600 to 2000 UT. ACE was located at (224, −20, 3) R_E GSM. These data were time-shifted by 50 min assuming radial propagation. Our assumption of radial propagation is justified by two considerations. First, the field direction was not predominantly in B_X, which reduces the uncertainty in arrival time of a particular IMF orientation. Second, ACE was close to the Sun-Earth line ($Y_{GSM} \sim -20$ R_E), which reduces radial propagation uncertainty to a few minutes. The IMF B_X was predominantly negative, while B_Y was positive for most of the interval plotted. The IMF B_Z was mostly negative before a northward turning at ∼1830 UT. The solar wind velocity varied between 475 and 500 km s^{-1}. The dynamic pressure was less than nominal at ∼1 nPa but increased to ∼1.75 nPa around 1800 UT. At this time the IMAGE magnetometer array [*Lühr et al.*, 1998] was located at ∼2200 LT. The geographic X (north-south) component of the magnetic field from six IMAGE stations is shown in Figure 7a. A moderate substorm onset was observed at IMAGE at 1806 UT at all the stations plotted. The geographic locations of the IMAGE stations are shown in Figure 7b. Included in the figure are the poleward and equatorward boundaries of a nominal auroral oval determined with the mathematical representation of *Holzworth and Meng* [1975]. We have used the Orbital Visualization Tool (OVT) of the Swedish Institute of Space Physics to map the geographic footpoints of the Cluster spacecraft using the Tsyganenko 1996 geomagnetic field model [*Tsyganenko*, 1995] for the appropriate solar wind IMF and dynamic pressure inputs (Figure 6). The four open squares plotted in Figure 7b indicate the footpoints of Cluster 3 at 1730, 1750, 1810, and 1830 UT. The Cluster footprints were located equatorward of the equatorward boundary of the nominal (but possibly not actual) auroral oval. The Cluster 3 footpoint mapped ∼30° east of IMAGE to northern Russia, from which ground magnetometer data were not available.

[19] Figure 8 shows the Cluster FGM and CIS/CODIF observations from 1700 to 1900 UT on 13 September 2002. The IMAGE substorm onset (1806 UT) is marked. There are no Cluster 2 CIS/CODIF data, and Cluster 3 CIS/CODIF data quality is poor at this time. There is a data gap in the FGM data from 1739 to 1743 UT. The proton number density (Figure 8f) shows that the spacecraft were in the plasma sheet ($n > 0.1$ cm^{-3}) for most of the interval plotted. The four spacecraft were north of the neutral sheet until ∼1735 UT, after which the neutral sheet repeatedly crossed Cluster 3. At the time of the substorm onset at IMAGE (1806 UT) the character of the Cluster FGM and CIS/CODIF observations noticeably changed. Despite the separation of the Cluster footpoints and the IMAGE network at this time (Figure 7b), the substorm produced a nearly instantaneous response at Cluster and IMAGE at 1806 UT. All three components of the magnetic field at Cluster (Figures 8a, 8b, and 8c) became disturbed and Cluster 1 and 4 began to observe strong tailward flows in excess of 600 km s^{-1} (Figure 8e). At the same time, Cluster 3 observed strong positive B_Y perturbations ($\Delta B_Y \sim 5-10$ nT), while Cluster 1, 2, and 4 observed strong negative B_Y perturbations ($\Delta B_Y \sim 5-10$ nT), although the B_Y component of the background magnetic field remained positive ($B_Y \sim 5-10$ nT). At the location of Cluster (Figure 5a) the background B_Y should be weakly negative in the northern hemisphere from flaring alone. The positive background B_Y observed from 1700 to 1900 UT may suggest some warping of the magnetotail due to the positive IMF B_Y [e.g, *Cowley and Hughes*, 1983]. However, we interpret the strong B_Y perturbations observed during the earthward and tailward flows as evidence of Hall current perturbations produced by magnetic reconnection at a near-Earth neutral line [*Sonnerup*, 1979; *Nagai et al.*, 2001], since these perturbations are rapid and larger than the background B_Y observed concurrently. At 1806 UT, the local B_Z at all four spacecraft turned abruptly negative with perturbations of 7–8 nT. The strong tailward flows accompanied with negative B_Y and B_Z perturbations in the northern plasma sheet are consistent with the Hall current structure and magnetic reconnection geometry on the tailward side of a neutral line ($-B_Z$). Cluster 3, south of the neutral sheet, observed a strong positive B_Y perturbation and the spacecraft north of the neutral sheet observed negative B_Y perturbations, consistent with the expected structure of perturbations produced by the Hall current (Figure 8i). Beginning at ∼1818 UT, Cluster 4 observed strong earthward flows ($V_X \sim 500$ km s^{-1}) north of the neutral sheet accompanied by positive B_Y and B_Z perturbations. At the same time Cluster 1 briefly continued to observe tailward flows of ∼200 km s^{-1}, which is puzzling considering the earthward location of Cluster 1 relative to Cluster 4 and may indicate small-scale structure in the flows. Cluster 1 observed earthward flow beginning at ∼1823 UT with positive B_Y and B_Z perturbations. At ∼1838 UT, Cluster 1 and 4 observed earthward flows approaching 800 km s^{-1}. These flows were accompanied by strong positive B_Y and B_Z perturbations. These observations are consistent with a position near the earthward side of a neutral line. The magnetic and flow observations from 1806 to 1900 UT at Cluster are consistent with the tailward passage and retreat of a near-Earth neutral line. By ∼1900 UT the substorm was nearing the recovery phase and the Cluster FGM and CIS/CODIF observed less disturbed conditions.

[20] Figure 9 shows the parameters of a time-varying Harris current sheet description for this event. The time range is the same as that for Figure 8, 1700–1900 UT on 13 September 2002. The substorm onset at 1806 UT is indicated. Figure 9a shows that the square of the lobe magnetic field B_0 increased slightly from ∼750 nT^2 to ∼900 nT^2 in the 30 min before the onset at 1806 UT, consistent with flux loading of the magnetotail during the substorm growth phase. As discussed previously, Cluster was well within the plasma sheet ($B_X \sim 0.5B_0$, inferred as ∼0.5 R_E above the current sheet midplane) and the current density J_Y was 3–5 nA m^{-2}. The total current sheet thickness (Figure 9d) gradually decreased from ∼4 R_E at 1700 UT to ∼1 R_E by 1806 UT. At 1806 UT, B_0^2 decreased by ∼400 nT^2 over ∼15 min and the magnetic

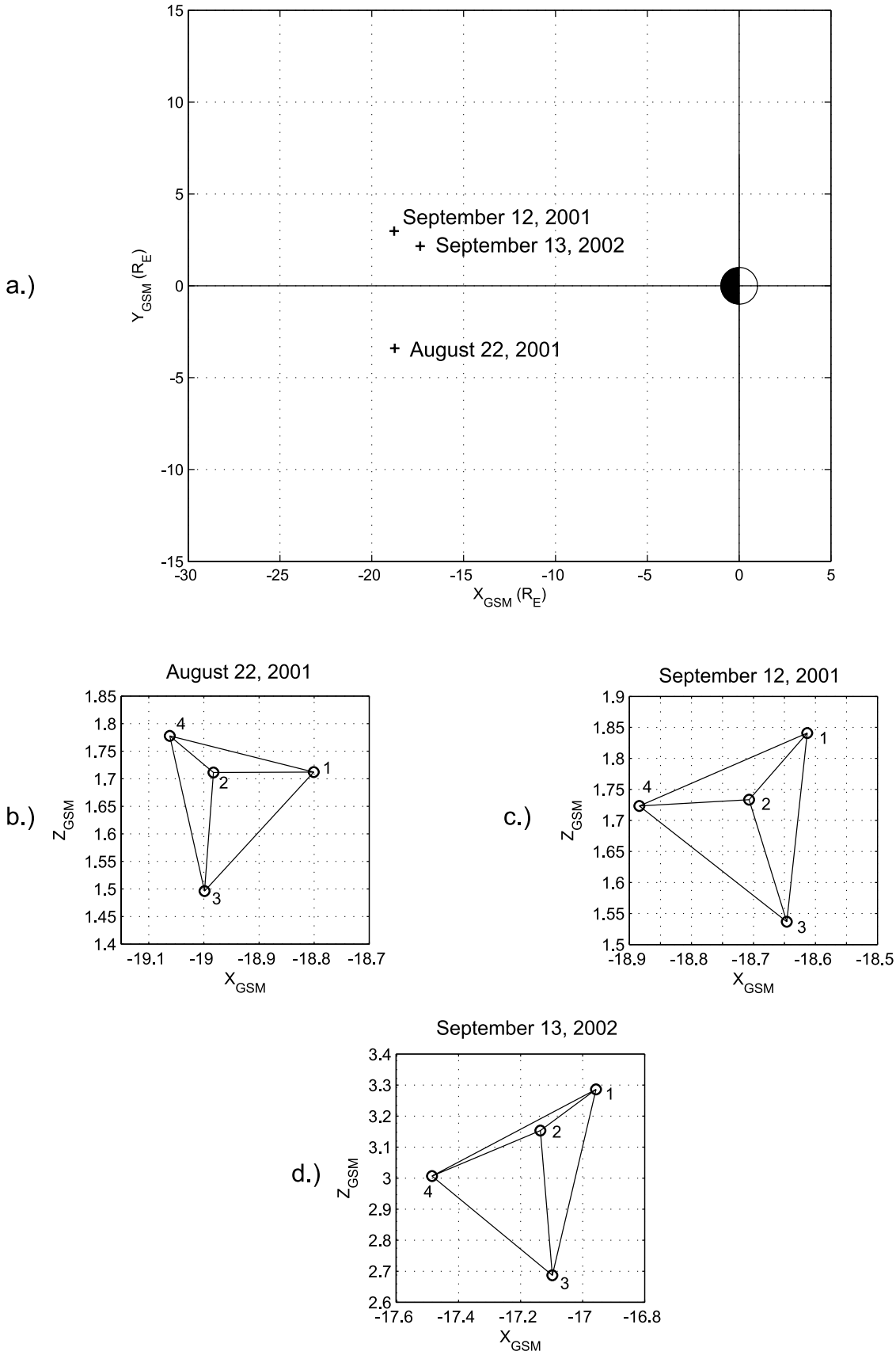

Figure 5. X-Y GSM location of Cluster and spatial orientations of the four spacecraft at the time of ground Pi2 onset for substorms on 22 August 2001, 12 September 2001, and 13 September 2002.

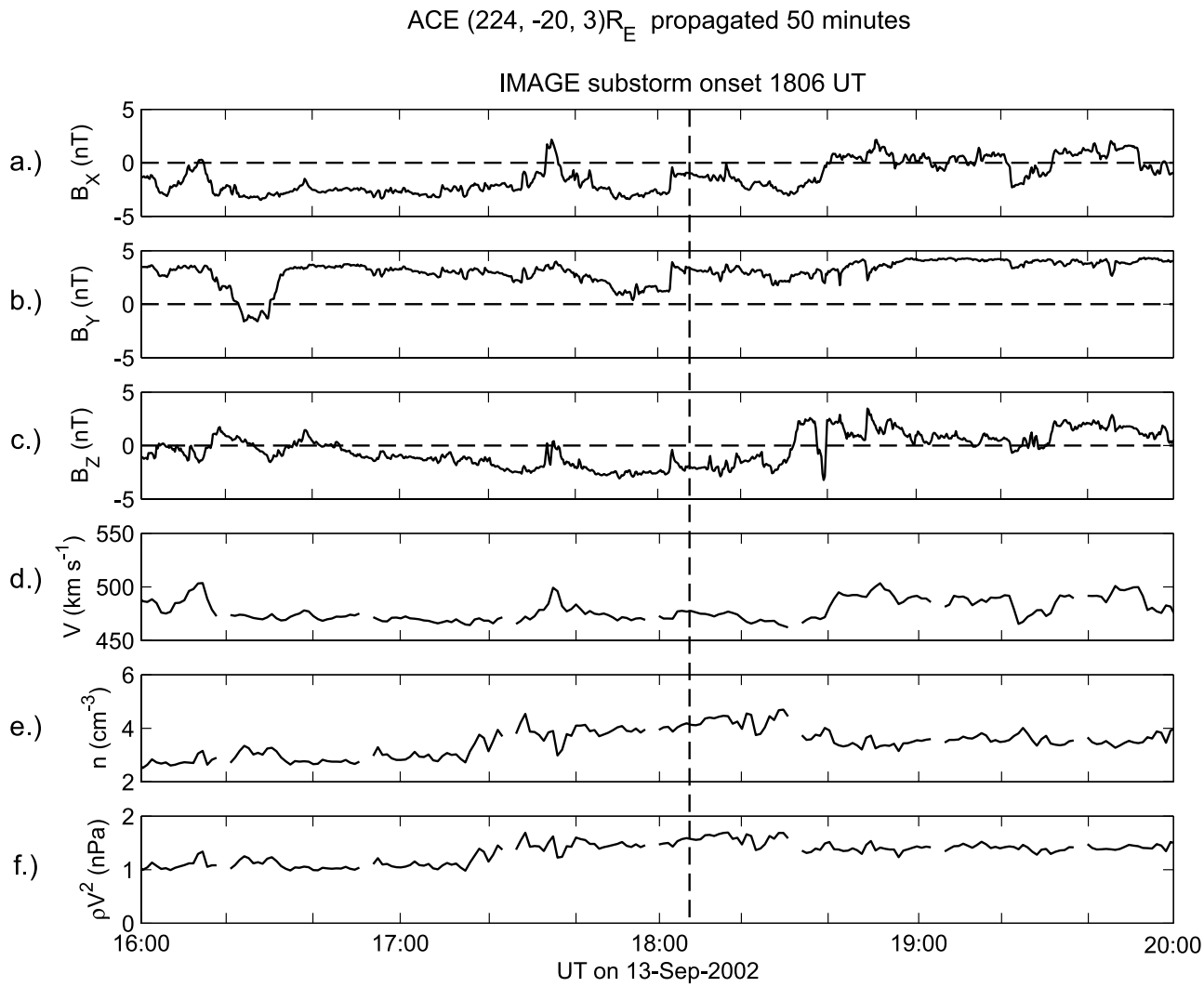

Figure 6. Solar wind observations from ACE on 13 September 2002, 1600–2000 UT in GSM coodinates. These data have been time-shifted by 50 min to account for propagation delay. The vertical dashed line indicates a substorm onset at the IMAGE magnetometer array. (a) B_X, (b) B_Y, (c) B_Z, (d) flow speed V, (e) number density n, (f) dynamic pressure.

field and current density became disturbed. The decrease in the lobe magnetic field B_0 appears to be a signature of the substorm onset at Cluster's position. Reconnection at the neutral line could account for the decrease in lobe magnetic field. At 1806 UT, Cluster 1 and 4 began observing strong tailward flows (Figure 8e) and negative B_Z (Figure 8c). The total current sheet thickness remained steady at $\sim$1 R_E after the substorm onset until $\sim$1820 UT. The $\sim$1 R_E total thickness is much larger than the proton inertial length in the current sheet ($\sim$500 km for n = 0.2 cm^{-3}) and approximately twice the proton gyroradius in the current sheet ($\sim$3500 km for a 5 keV proton in a 2 nT magnetic field). Cluster began observing strong earthward flows and positive B_Z perturbations at $\sim$1820 UT. As the substorm progressed after 1830 UT, the total current sheet thickness increased to $\sim$3–4 R_E and fluctuated around this level for the remainder of the time shown in the figure. Despite the substorm onset, the current sheet position parameter Z-z_0 (Figure 9e, thick black trace) remained remarkably close to the Hammond prediction (thin black trace) from 1730 to 1830 UT. The agreement was less satisfactory after 1830 UT during the recovery phase. The Hammond model [*Hammond et al.*, 1994] provides the nominal position of the current sheet, dependent on dipole tilt and solar wind dynamic pressure only. As a result, the Hammond model cannot represent the local warping of the current sheet that may occur during substorms.

[21] The time-varying Harris thickness results for this event are consistent with the expected average changes in the plasma sheet during a substorm [e.g., *Baumjohann et al.*, 1992]. The lobe magnetic field increased and the current sheet thickness decreased during the nominal growth phase. Although this signature could appear in the absence of a substorm (e.g., there is an increase in solar wind dynamic pressure around 1730 UT that could compress the magnetosphere and cause B to increase in the lobe (Figure 6f)), the close association of both magnetic field increase and decrease with a ground onset at IMAGE is suggestive. Cluster observed the magnetic field and the flow signatures

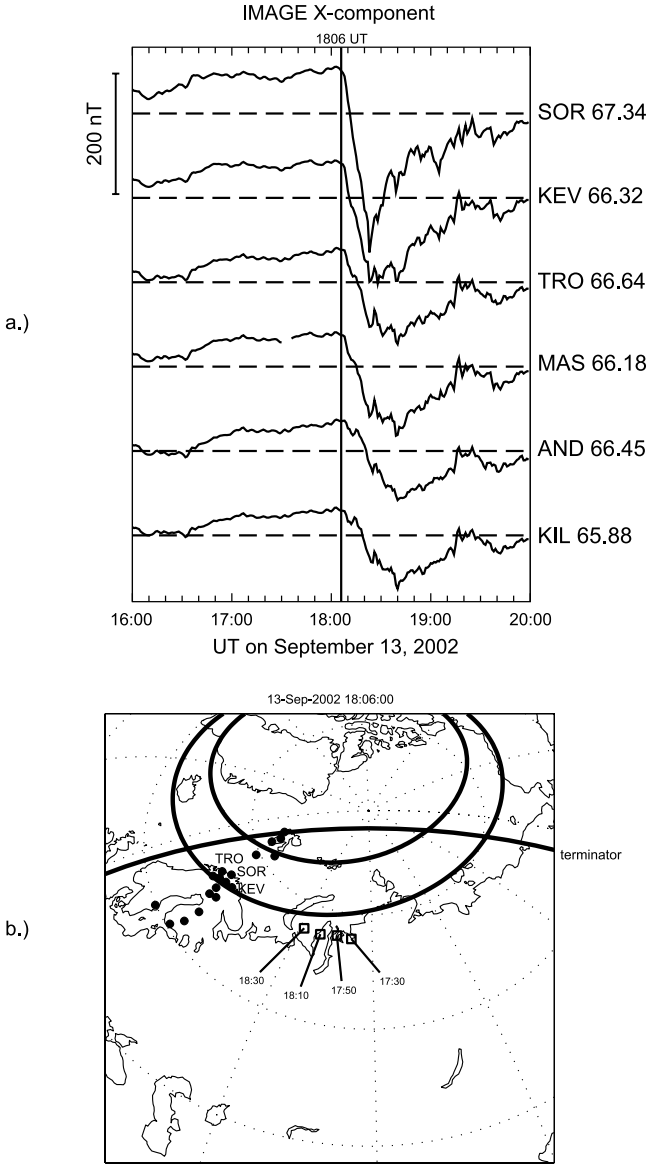

Figure 7. (a) Geographic X-component of the magnetic field at six stations of the IMAGE magnetometer network on 13 September 2002 1600–2000 UT. A moderate substorm onset was observed at ~1806 UT. The corrected geomagnetic (CGM) latitude of each station is indicated next to the station name abbreviation. (b) Geographic locations of the ground stations of the IMAGE magnetometer network as well as footpoints of Cluster 3. See text for further details.

of a neutral line beginning at 1806 UT. Based on the flows, the neutral line was first located earthward of the spacecraft (tailward flows) and then passed tailward of the spacecraft (earthward flows). Despite the ~5000 km separation of the Cluster spacecraft at this time, all four spacecraft measured similar magnetic field and flow signatures and found evidence for the Hall current system.

5.2. The 12 September 2001 Event

[22] For our second case study substorm, Cluster was located at (−18.7, 3, 1.62) R_E GSM at 1300 UT on 12 September 2001. The orientation of the tetrahedron in the X-Z plane is shown in Figure 5c. Figure 10 shows ACE solar wind observations for the time interval 1100–1500 UT. The plot format is identical to Figure 6. ACE was located at (229, −32, 17) R_E GSM and with an average solar wind speed of 375 km s^{-1} the radial propagation delay to the nose of the magnetosphere was calculated to be 65 min. As with the first substorm event, the roughly spiral magnetic field orientation and the location of ACE close to the Sun-Earth line make it reasonable to adopt purely radial propagation of the solar wind parameters. The IMF B_X was negative for most of the interval, fluctuating around −5 nT. The IMF B_Y was almost entirely positive, with values between 3 and 5 nT. The IMF B_Z was mostly negative (~−4 nT). The solar wind bulk speed decreased from ~425 km s^{-1} between 1100 and 1200 UT to ~375 km s^{-1} between 1200 and 1500 UT. The solar wind proton number density fluctuated around 4 cm^{-3} and the dynamic pressure was ~1 nPa.

[23] Stations of the 210 Magnetic Meridian were located at ~2300 LT at 1300 UT on 12 September 2001. The H (north-south) component of the magnetic field from the northern 210MM stations TIK and CHD are shown in Figure 11a. A small substorm onset (~150 nT) was observed at both TIK and CHD at ~1309 UT. The geographic locations of these two stations are shown in Figure 11b, along with the geographic footpoints (open squares) of Cluster 3 at 1230, 1250, 1310, and 1330 UT mapped with the OVT Tsyganenko 1996 magnetic field model for appropriate solar wind IMF and dynamic pressure inputs (Figure 10). The nominal auroral oval of Holzworth and Meng has been mapped. As with our previous example, the footpoints of Cluster 3 mapped to northern Russia. The Cluster 3 footpoints and the ground stations TIK and CHD were located near the equatorward boundary of the nominal auroral oval.

[24] Cluster FGM and CIS/CODIF observations from 1200 to 1400 UT on 12 September 2001 are shown in Figure 12 in the same format as Figure 8. The substorm onset at TIK and CHD at 1309 UT is indicated. At 1200 UT all four spacecraft were clearly in the northern plasma sheet (B_X ~ 20 nT, n ~ 0.25 cm^{-3}) and remained within the plasma sheet for most of the interval plotted. Just after 1230 UT the neutral sheet crossed Cluster 3 repeatedly (Figure 12a). The neutral sheet also briefly crossed Cluster 2 and 4 at ~1238 UT. The neutral sheet crossed back over Cluster 2 and 4 at ~1242 UT but remained close to Cluster 3 until ~1340 UT. The B_Y magnetic field was small and positive (~3 nT) at 1200 UT but increased to nearly 10 nT at ~1218 UT (Figure 12b). We expect negative

Figure 8. Cluster FGM and CIS/CODIF observations on 13 September 2001 1700–1900 UT in GSM coordinates. FGM data from all four Cluster spacecraft are plotted while CIS/CODIF data are plotted for Cluster 1 and 4. The vertical black line indicates the substorm onset at IMAGE. (a) B_X, (b) B_Y, (c) B_Z, (d) B, (e) V_X, (f) V_Y, (g) V_Z, (h) proton number density n, (i) neutral line schematic for the geometry of the magnetotail. See color version of this figure at back of this issue.

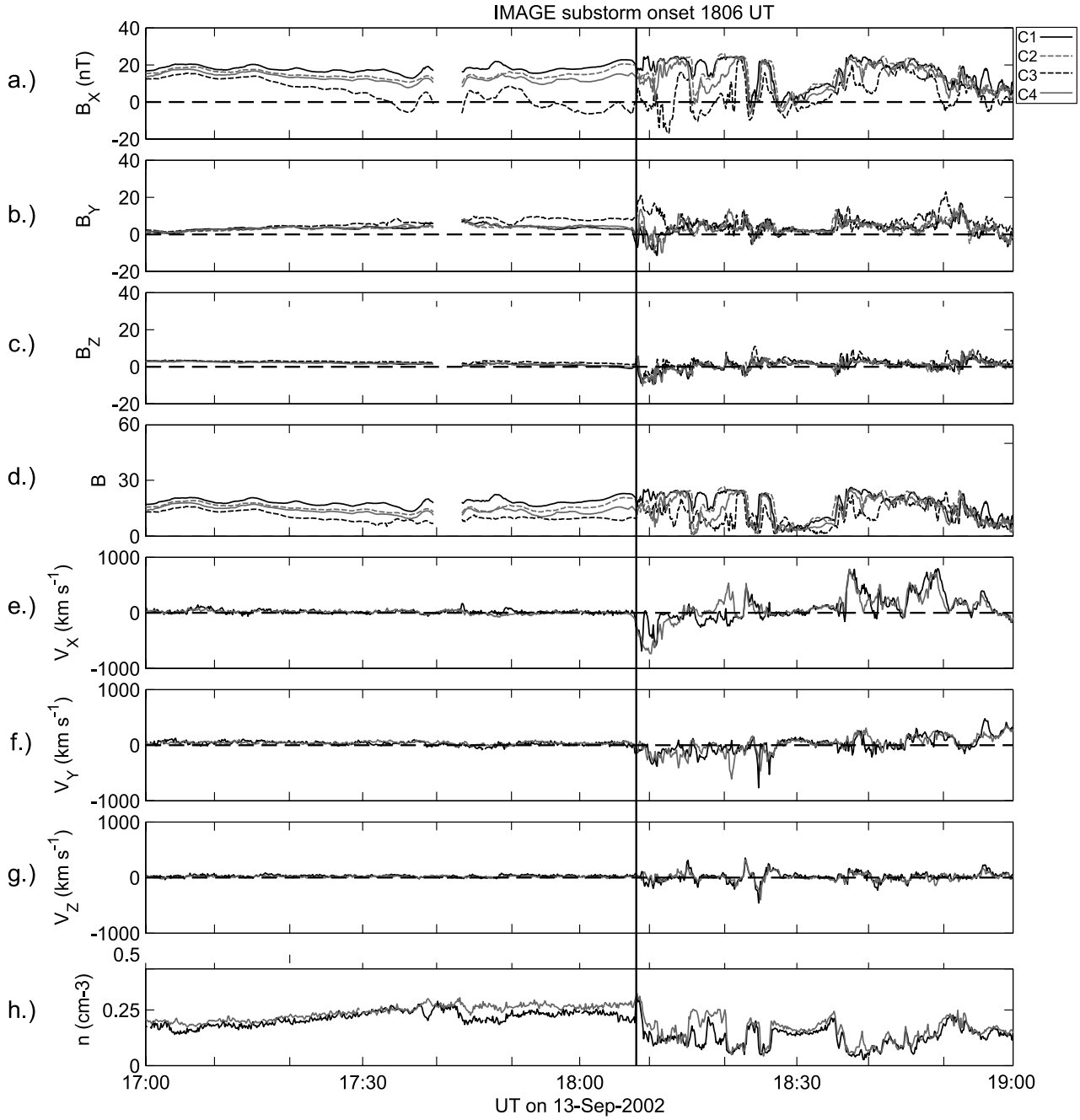
IMAGE substorm onset 1806 UT
a.)
b.)
c.)
d.)
e.)
f.)
g.)
h.)
i.)
C1
C2
C3
C4
B_X (nT)
B_Y
B_Z
B
V_X (km s^{-1})
V_Y (km s^{-1})
V_Z (km s^{-1})
n (cm-3)
17:00
17:30
18:00
18:30
19:00
UT on 13-Sep-2002
inflow
X-line
outflow
Hall current
Hall current
B_Y
B_Y
Z
X
Y

Figure 8

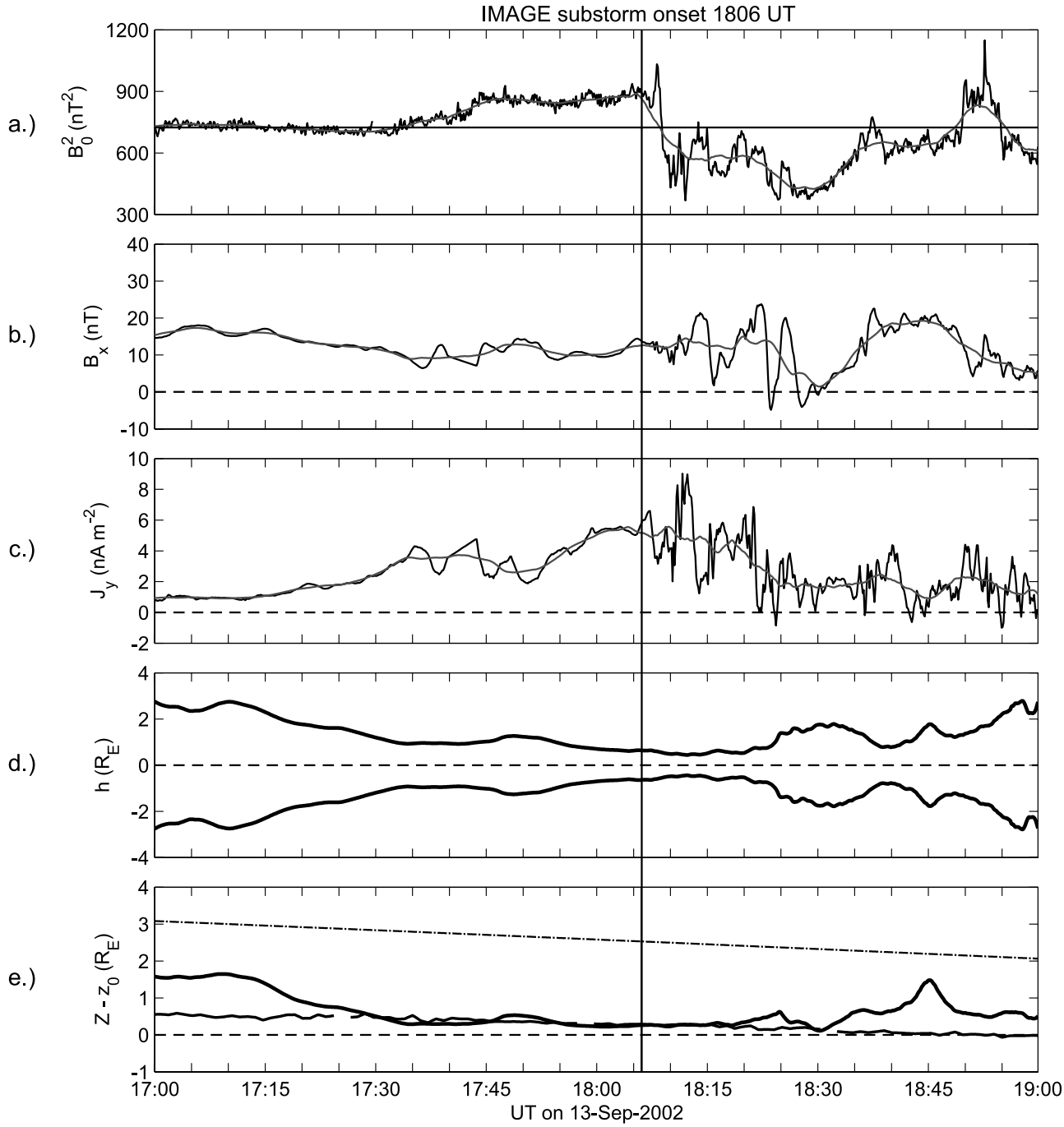

Figure 9. Temporal variation of current sheet thickness and position for the plasma sheet crossing of 13 September 2002, 1700–1900 UT. (a) $B_0{}^2$, square of the lobe magnetic field and 6-min running average (gray). The horizontal black line shows a baseline to emphasize the growth phase increase of B_0, (b) four-spacecraft averaged B_X (black) and 6-min running average (gray), (c) J_Y and 6-min running average (gray), (d) current sheet half-thickness h plotted with a mirror image to indicate the total thickness cross-section, (e) Cluster position relative to current sheet (Z-z_0), Cluster Z position (dash-dot trace), and predicted Cluster position relative to current sheet from the *Hammond et al.* [1994] model (thin black trace). The Hammond model predicts the current sheet cross-section at fixed X based on dipole tilt and solar wind dynamic pressure. The gaps in the Hammond model prediction trace correspond to data gaps in the dynamic pressure time series input.

background B_Y in the northern premidnight plasma sheet from flaring alone. This was not observed, suggesting that the strong positive B_Y of the solar wind penetrated the magnetotail. Between 1200 and 1300 UT, Cluster was located on the closed field lines of the nightside plasma sheet with B_Z positive (Figure 12c). There were no strong flows between 1200 and 1300 UT. Disturbances of the magnetic field and the flow began at ~1305 UT. High-frequency

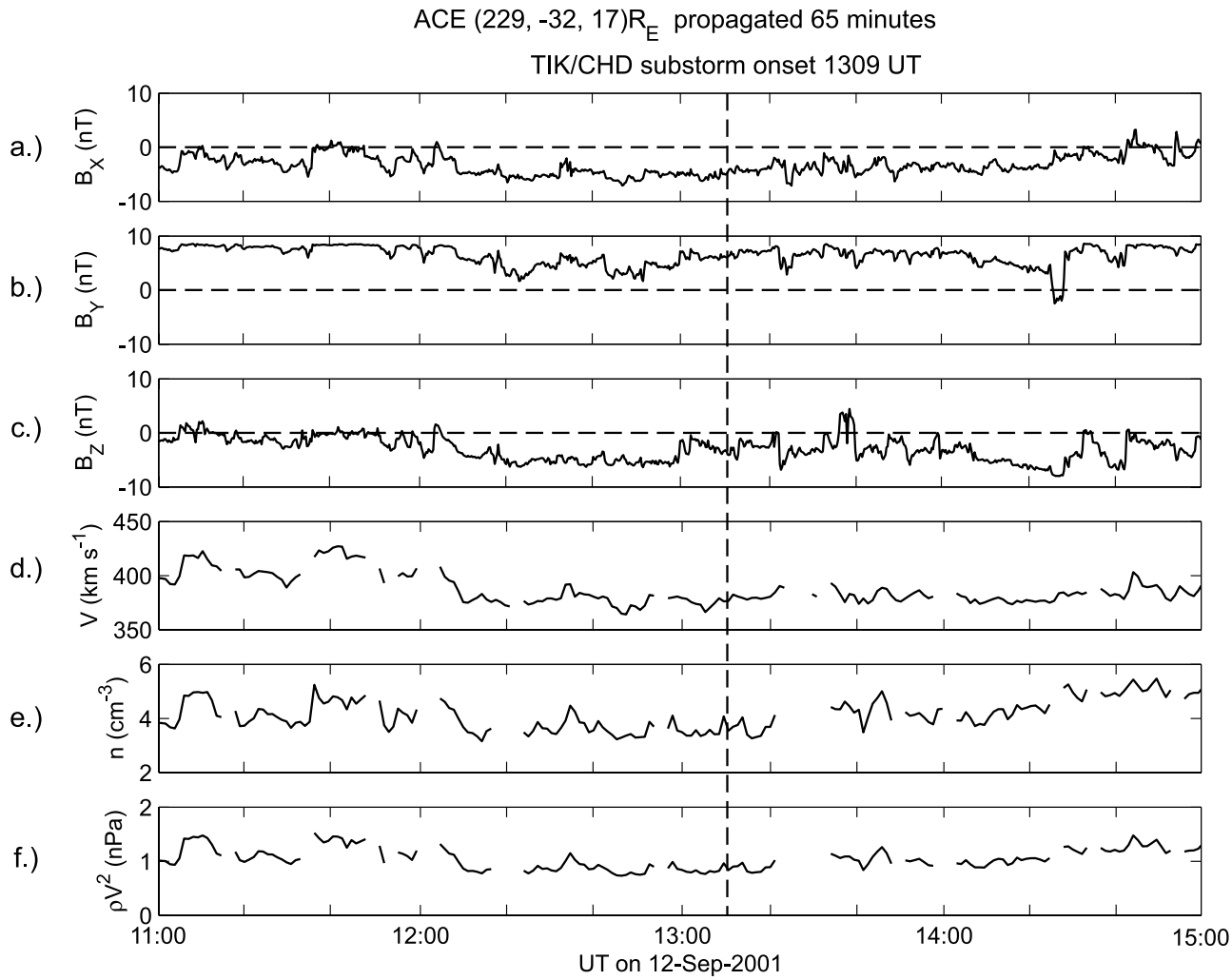

Figure 10. Solar wind observations from ACE on 12 September 2001, 1100–1500 UT in GSM coordinates. These data have been time-shifted by 65 min to account for propagation delay. The vertical black line indicates a substorm onset at the 210 Magnetic Meridian stations TIK and CHD. (a) B_X, (b) B_Y, (c) B_Z, (d) flow speed V, (e) number density n, (f) dynamic pressure.

fluctuations in the magnetic field were accompanied by the onset of tailward flows of ~200 km s^{-1} at Cluster 3 (Figure 12e). The flows at Cluster 3 then turned alternately earthward and tailward for the next 15 min with a periodicity of ~3–4 min. The earthward flows were generally larger than the tailward flows at Cluster 3. Weaker flows were present at Cluster 1 and 4. The flows turned strongly earthward at Cluster 3 at ~1310 UT with a magnitude of 800 km s^{-1}. Bursty earthward flows reaching nearly 1000 km s^{-1} between 1315 and 1325 UT were measured at Cluster 1, 3, and 4. During this time, there were strong dawnward ($-V_Y$) flows exceeding 600 km s^{-1} at Cluster 1, 3, and 4 (Figure 12f). In addition, brief positive perturbations as large as ~15 nT in B_Y and B_Z often exceeded the background level of these components. Although the magnetic field and the flows are quite complicated on small timescales, positive B_Y (Hall current magnetic perturbation) and B_Z perturbations accompanied by earthward flows in the northern plasma sheet are consistent with the passage of a neutral line by Cluster. The strong dawnward flows are unusual in the onset phase of a substorm (Figure 12f). Possibly the neutral line was not orthogonal to the Earth-Sun line and the outflow regions produced earthward and dawnward flows or perhaps there were multiple neutral lines of limited cross-tail extension. The substorm onset signature arrived at the ground stations TIK and CHD at 1309 UT just a few minutes after the onset of disturbed magnetic field and strong flows at Cluster (~1305 UT).

[25] Figure 13 shows the time-varying Harris model parameters for this substorm interval. The plot format is analogous to Figure 9 except that a sixth panel has been added showing the auroral indices *AU*, *AL*, and *AE* (Figure 13f). The substorm onset at TIK and CHD is indicated. At 1200 UT the full thickness of the current sheet was ~6–7 R_E (Figure 13d) and Cluster was located within the plasma sheet ($B_X \sim 0.7B_0$). Between 1215 and 1300 UT, the lobe magnetic field B_0^2 increased from 600 to ~800 nT^2 (Figure 13a). The full thickness of the current sheet gradually decreased from ~3 R_E to ~1 R_E from 1215 to 1300 UT. At ~1303 UT the lobe magnetic field abruptly began to decrease, reaching a minimum of ~200 nT^2 at 1330 UT. Concurrently, Cluster began to measure disturbed magnetic

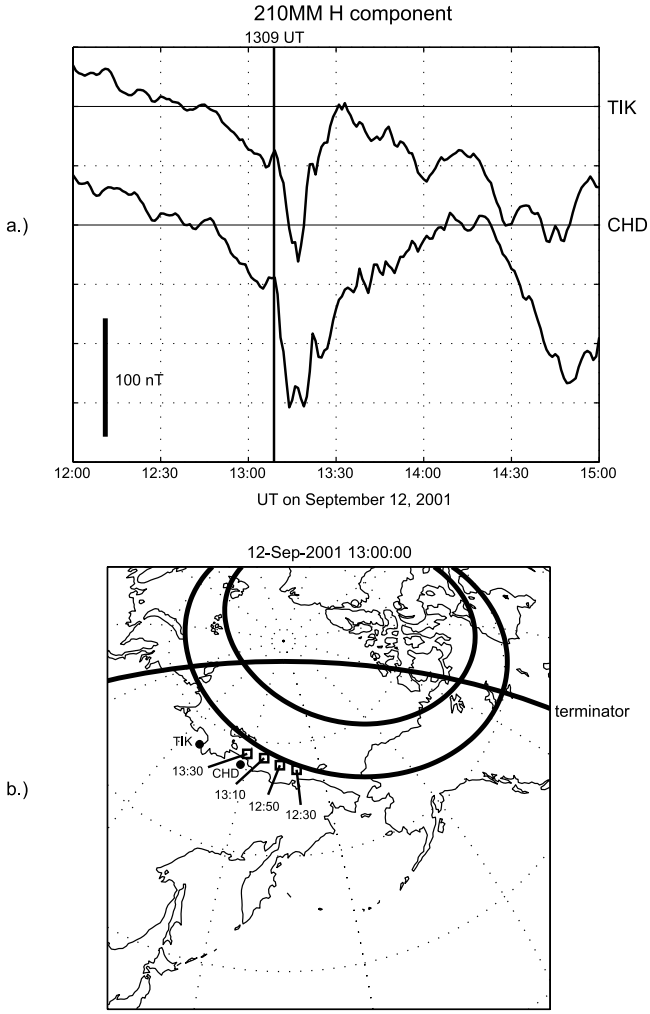

Figure 11. (a) Geographic X-component of the magnetic field at TIK and CHD stations of the 210 Magnetic Meridian on 12 September 2001 1200–1500 UT. A moderate substorm onset was observed at 1309 UT at TIK and CHD. (b) Geographic locations of the ground stations TIK and CHD as well as footpoints of Cluster 3.

field and flows. Thus 1305 UT may be identified as the local onset of the substorm at Cluster. The minimum of the full current sheet thickness of $\sim$0.8 R_E was reached at $\sim$1308 UT. The thickness at this time was larger than a proton inertial length ($\sim$500 km) but only slightly larger than the proton gyroradius ($\sim$3500 km) in the current sheet. At 1308 UT signatures consistent with the passage of a neutral line (Figure 12) were present. Between 1315 and 1330 UT the full thickness of the current sheet rapidly increased from less than an R_E to 6–7 R_E before thinning again to $\sim$4 R_E by 1345 UT, roughly at the time of a secondary decrease of *AL*. The time-varying current sheet position Z-z_0 matched the Hammond model prediction only between 1230 and 1245 UT, which may indicate the model was less reliable when the magnetotail became very disturbed.

5.3. The 22 August 2001 Event

[26] We now discuss an event on 22 August 2001 for which the time-varying Harris model gives parameters that show less agreement with the phenomenological predictions of the near-Earth neutral line (NENL) model of substorms [*McPherron et al.*, 1973; *Russell and McPherron*, 1973; *McPherron*, 1991]. The time-varying Harris model analysis of the substorm onsets identified on 12 September 2001 and 13 September 2002 was generally consistent with the expectations of the NENL model. The lobe magnetic field increased during the growth phase, then decreased at the time of the onset of the substorm at Cluster. A thin current sheet was present during both events. The FGM and CIS/CODIF observations were consistent with the passage of a neutral line.

[27] On 22 August 2001 at 1000 UT Cluster was located at (−18.7, −3.4, 1) R_E GSM. ACE observations between 0800 and 1200 UT are shown in Figure 14. ACE was located at (239, −26, 32) R_E GSM. The data were time-shifted by 44 min assuming radial propagation delay. We used an average solar wind speed of 575 km s^{-1} and the 239 R_E upstream position of ACE to calculate the delay. While ACE was located near the Sun-Earth line, the dominant IMF B_X between 0840 and 0910 UT introduces considerable uncertainty in our propagation delay. The alternating positive and negative B_Z between 0840 and 0910 UT also makes it difficult to establish the polarity of B_Z during this interval. The IMF B_X was strong and positive, B_Y was predominantly negative, and B_Z was predominantly positive before a strong southward turning at $\sim$0910 UT. Thereafter, the IMF remained southward for over 2 hours. The solar wind velocity was above average but the dynamic pressure was nominal at $\sim$2 nPa. At 0930 UT the stations of the CANOPUS magnetometer array, located in the midnight local time sector, observed the onset of a moderate substorm. The geographic X (north-south) component of the magnetic field from six CANOPUS stations is shown in Figure 15a. The geographic locations of the CANOPUS stations are shown in Figure 15b. The footpoints of Cluster 3 at 0900, 0920, 0940, and 1000 UT are shown. The Cluster footpoints and the CANOPUS stations were located between the poleward and equatorward boundaries of the nominal auroral oval plotted. The Cluster 3 footpoint mapped close to the CANOPUS station FSMI between 0920 and 1000 UT. The main onset of a moderate substorm occurred at 0940 UT, most clearly at the westernmost stations DAWS and FSIM. A possible pseudo-breakup was observed at $\sim$0925 UT at GILL, RABB, and FSMI. On the basis of the mapping, we expect the substorm onset to be associated closely in time with evidence of substorm effects at Cluster.

[28] Figure 16 shows the FGM and CIS/CODIF data at Cluster from 0915 to 1030 UT. The main substorm onset at 0940 UT is indicated. Between 0915 and 0930 UT, Cluster was located well within the plasma sheet ($n \sim 0.25$ cm^{-3}) and the magnetic field magnitude began a gradual increase interrupted by a short-lived decrease just before 0930 UT (Figure 16d). The B_Y and B_Z components (Figures 16b and 16c plotted with scales that differ from Figure 16a) were $\leq$5 nT and there were no strong earthward or tailward flows. Between 0930 and 0940 UT, Cluster B_X was $\sim$30 nT and the densities slowly decreased reaching a level of $n \sim 0.2$ cm^{-3} typical of the plasma sheet boundary layer. The pseudo-breakup around 0925 UT is associated with negative B_Z at all four spacecraft and brief tailward flows at Cluster 3

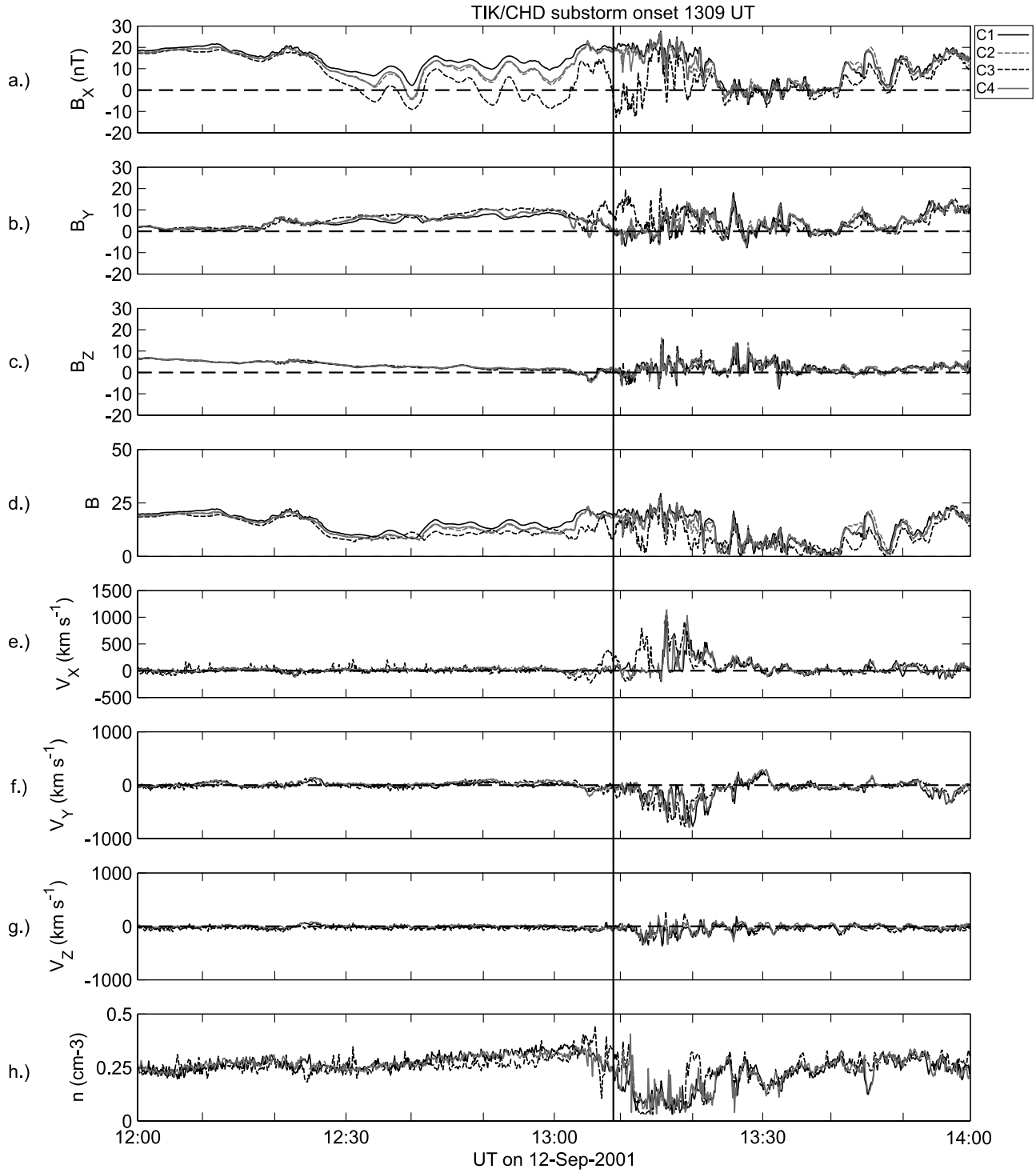

Figure 12. Cluster FGM and CIS/CODIF observations on 12 September 2001, 1200–1400 UT in GSM coordinates. FGM data from all four Cluster spacecraft are plotted while CIS/CODIF data are plotted for Cluster 1, 3, and 4. The vertical black line indicates the substorm onset at TIK and CHD. (a) B_X, (b) B_Y, (c) B_Z, (d) B, (e) V_X, (f) V_Y, (g) V_Z, (h) proton number density n. See color version of this figure at back of this issue.

(Figure 16e). At 0940 UT, the time of the main onset at FSIM and DAWS, Cluster observed substantial changes in the magnetic field and flow. The neutral sheet moved northward rapidly, crossing first Cluster 3 and Cluster 1, 2, and 4 a few minutes later (see Figure 5b). The B_Y perturbations at Cluster 3 were in antiphase with those at Cluster 1, 2, and 4, and B_Z increased at all four spacecraft. At the same time, strong earthward flows ($+V_X$) appeared first at Cluster 3 and then at Cluster 1 and Cluster 4. A few minutes later the spacecraft observed strong tailward flows ($-V_X$) associated with a small negative B_Z. Starting at ~0955 UT, the flows shifted earthward again and B_Z

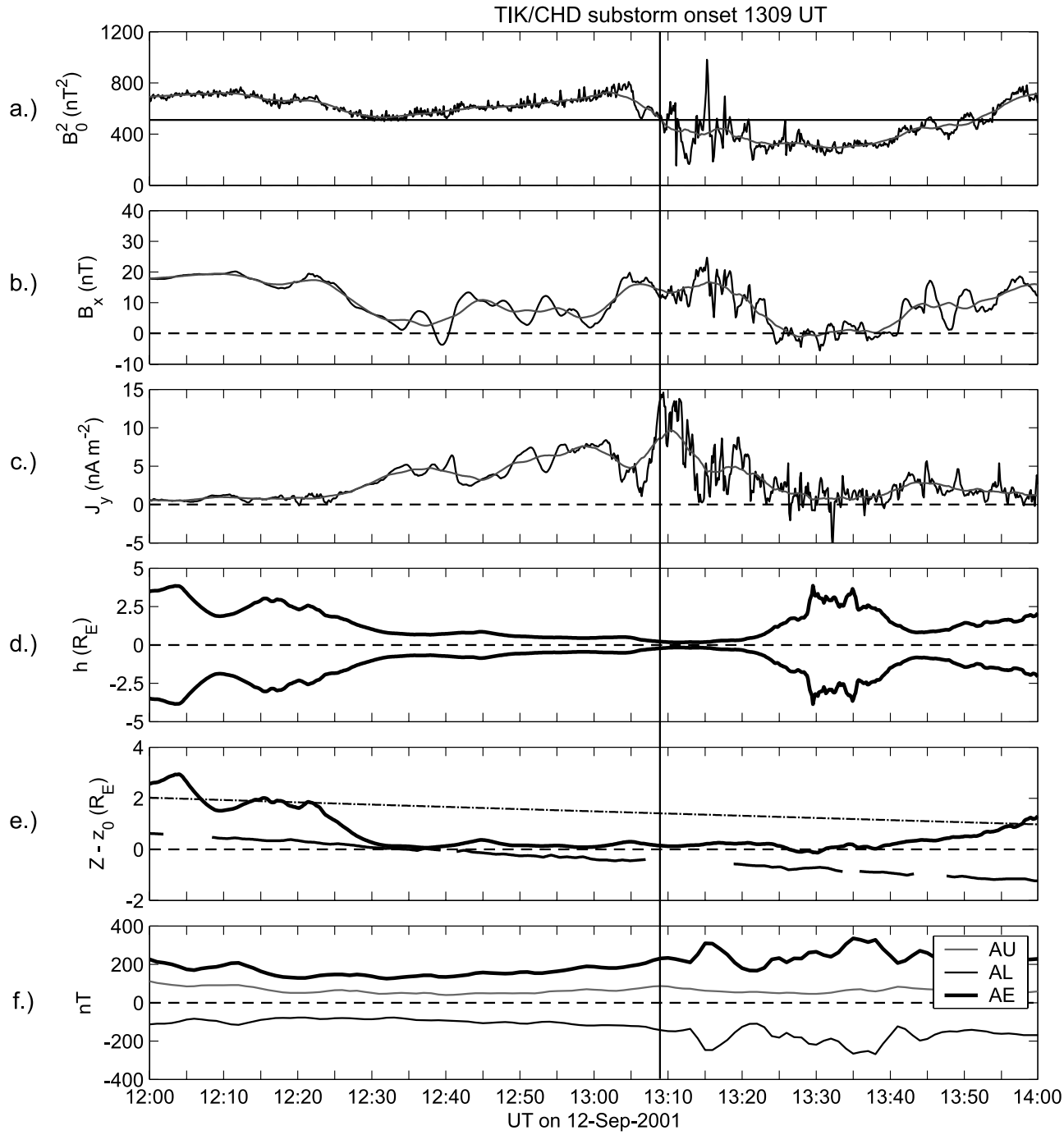

Figure 13. Temporal variation of current sheet thickness and position for the plasma sheet crossing of 12 September 2001, 1200–1400 UT. (a) $B_0{}^2$, square of the lobe magnetic field and 6-min running average (gray). The horizontal black line shows a baseline to emphasize the growth phase increase of B_0, (b) four-spacecraft averaged B_X (black) and 6-min running average (gray), (c) J_Y and 6-min running average (gray), (d) Current sheet half-thickness h plotted with a mirror image to indicate the total thickness cross section, (e) Cluster position relative to current sheet (Z-z_0), Cluster Z position (dash-dot trace), and predicted Cluster position relative to current sheet from the *Hammond et al.* [1994] model (thin black trace). (f) Auroral activity indices *AU*, *AL*, and *AE*.

became strongly positive at all four spacecraft. These observations are consistent with the passage of a neutral line over Cluster. Cluster 3 observed positive (negative) B_Y perturbations north (south) of the neutral sheet around 0940 UT. At the same time Cluster 1, 2, and 4 observed only a positive B_Y perturbation north of the neutral sheet. We interpret the B_Y perturbations as Hall current perturbations and not signatures of magnetotail flaring (positive (negative) B_Y in the northern (southern) lobe at the location of Cluster) because the background magnetic

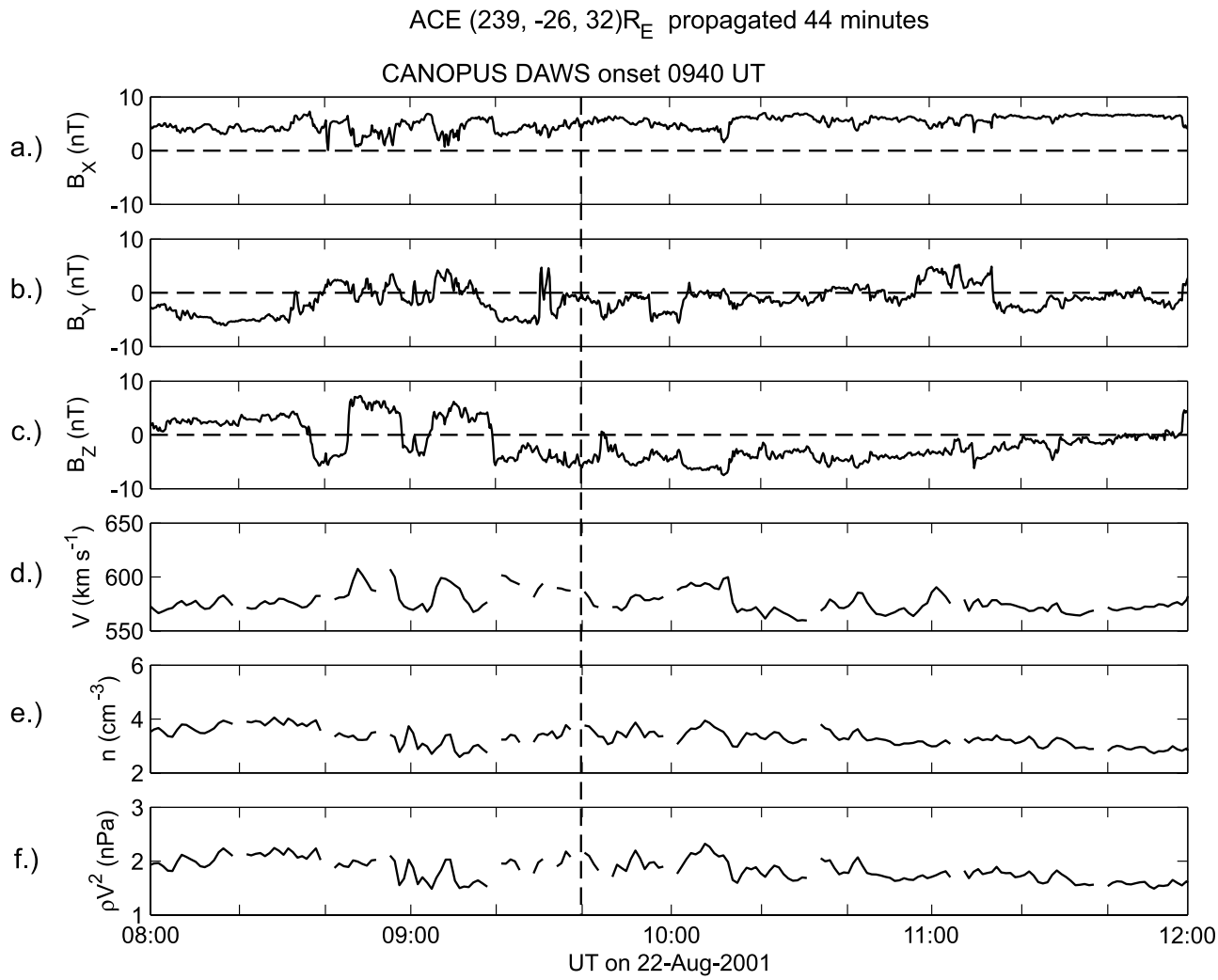

Figure 14. Solar wind observations from ACE on 22 August 2001, 0800–1200 UT in GSM coordinates. These data have been time-shifted by 44 min to account for propagation delay. A vertical dashed line indicates the main substorm onset at DAWS of the CANOPUS array. (a) B_X, (b) B_Y, (c) B_Z, (d) flow speed V, (e) number density n, (f) dynamic pressure.

field in the 10 min prior to the large B_Y perturbations at 0940 UT was very small. The positive B_Z during earthward flow and negative B_Z during tailward flows are consistent with locations on reconnected field lines on the earthward side of a neutral line or on a plasmoid on the tailward side of a neutral line, respectively.

[29] Figure 17 shows the time-varying Harris model fit from 0915 to 1030 UT. When the average current densities (gray trace in Figure 17c) fell below 0.3 nA m^{-2} (e.g., around 0935 UT), they were not used for estimates of parameters, leading to gaps in the traces of $h(t)$ and $Z\text{-}z_0(t)$ (Figures 17d and 17e). During the growth phase, between 0915 and 0940 UT, the total thickness of the current sheet was ~2–4 R_E and the lobe magnetic field B_0^2 (Figure 17a) increased from ~500 nT^2 to ~900 nT^2. However, the decrease of plasma sheet thickness typical of the growth phase of a substorm was not clearly observed. Local rapid increases in $h(t)$ at 0935 and 0937 UT occurred at times when Cluster was likely in the PSBL. The auroral current system of the substorm began to intensify at 0930 UT (Figure 17f). Strong earthward flows, increase of B_Z, and structured changes of B_Y in Figure 16 around 0940 UT are consistent with a neutral line passing across Cluster. The lobe magnetic field reached a minimum of ~400 nT^2 at ~0953 UT. The current sheet remained relatively thin at ~0.2–0.4 R_E until 1000 UT, at which time the thickness began to increase. The auroral indices indicate continuing activity. By 1020 UT the full thickness of the current sheet was ~5 R_E. The position of Cluster relative to the current sheet ($Z\text{-}z_0$) tracked predictions from the Hammond model. The Hammond model does not predict motions of the current sheet during substorms but did agree with the data quite well between 0945 and 1030 UT.

[30] Our results with the time-varying Harris thickness for this event are not entirely consistent with the nominal changes of the plasma sheet during a substorm. We did not observe plasma sheet thinning prior to the main substorm onset at CANOPUS at 0940 UT nor did we observe systematic changes following the local onset of activity at 0940 UT. Cluster observed the magnetic field and flow signature of a neutral line beginning at 0940 UT. This could result from the neutral line reaching the location of Cluster

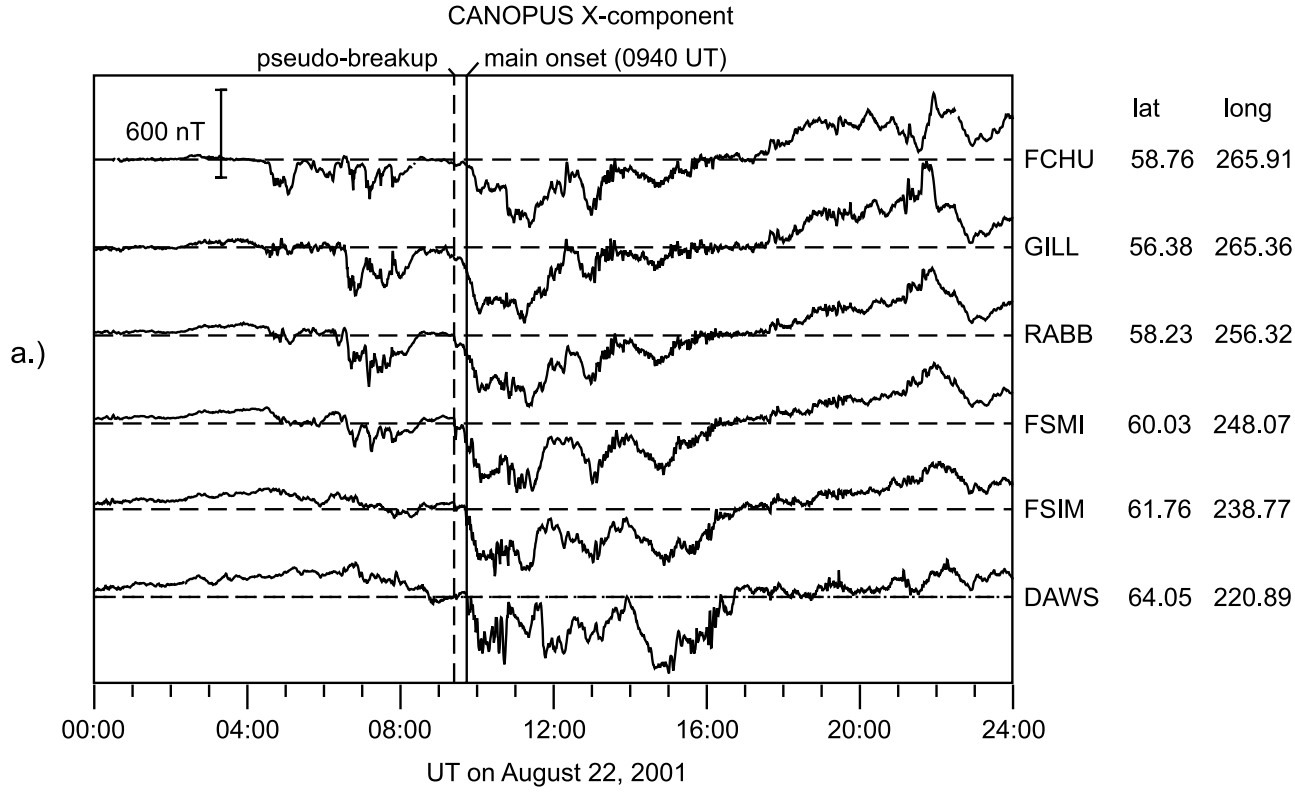

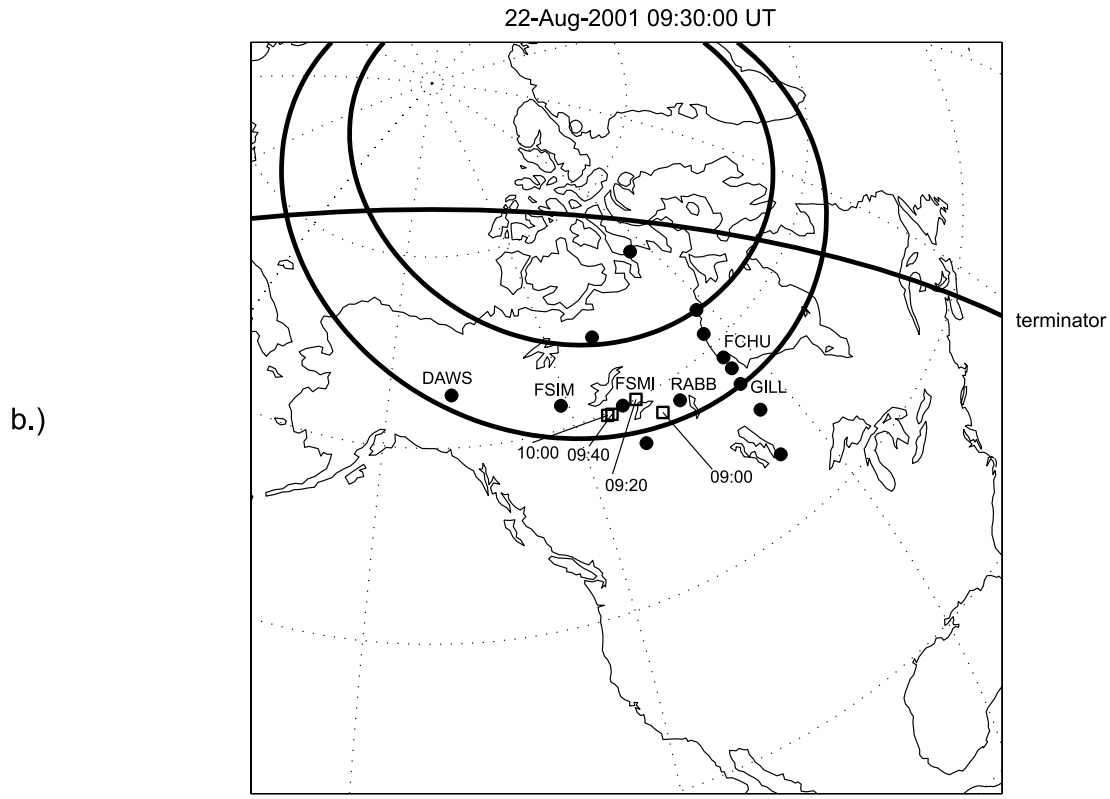

Figure 15. (a) Geographic *X*-component of the magnetic field at six stations of the CANOPUS magnetometer array on 22 August 2001, 0000–2400 UT. CANOPUS was located in the 0000–0200 LT sector and observed a substorm onset at 0940 UT, indicated by the vertical line. The geodetic latitude and longitude for each station is indicated with the station name abbreviation on the right. (b) Geographic locations of the CANOPUS stations as well as the mapped footpoints of Cluster 3.

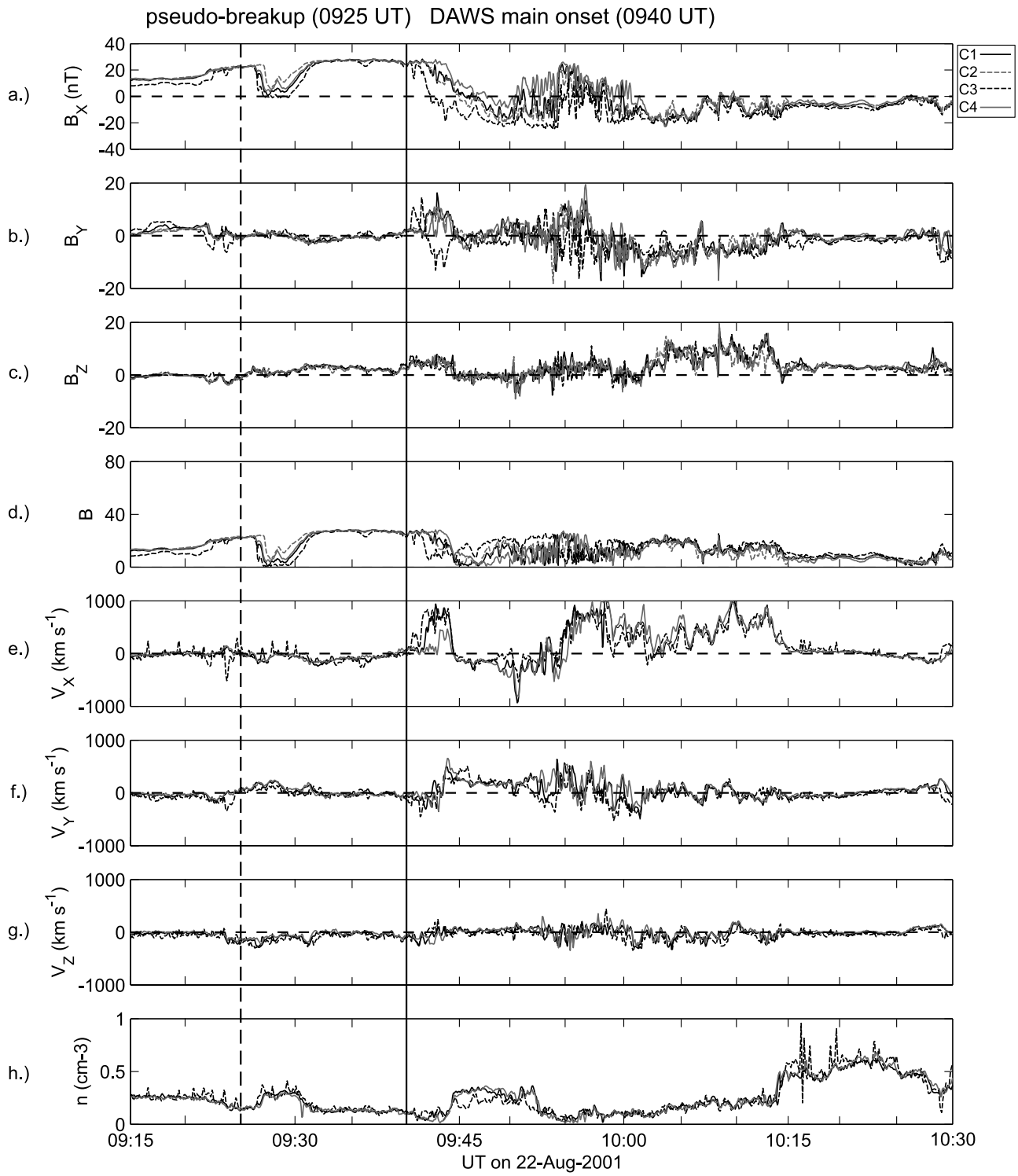

Figure 16. Cluster FGM and CIS/CODIF observations on 22 August 2001, 0915–1030 UT in GSM coordinates. FGM data from all four Cluster spacecraft are plotted while CIS/CODIF data are plotted for Cluster 1, 3, and 4. The vertical black line indicates the main onset at DAWS. The vertical dashed line indicates a likely pseudo-breakup. (a) B_X, (b) B_Y, (c) B_Z, (d) B, (e) V_X, (f) V_Y, (g) V_Z, (h) proton number density n. See color version of this figure at back of this issue.

at 0940 UT or Cluster may have detected an already active neutral line upon reentering the central plasma sheet from the PSBL at 0940 UT. When Cluster reentered the central plasma sheet at 0940 UT the thickness of the current sheet was ~2000 km, which is ~4 proton inertial lengths (~500 km) in the current sheet but less than a proton gyroradius ($\rho_i \sim 3500$ km). The thickness remained less than 1 R_E until 1000 UT, which is inconsistent with the

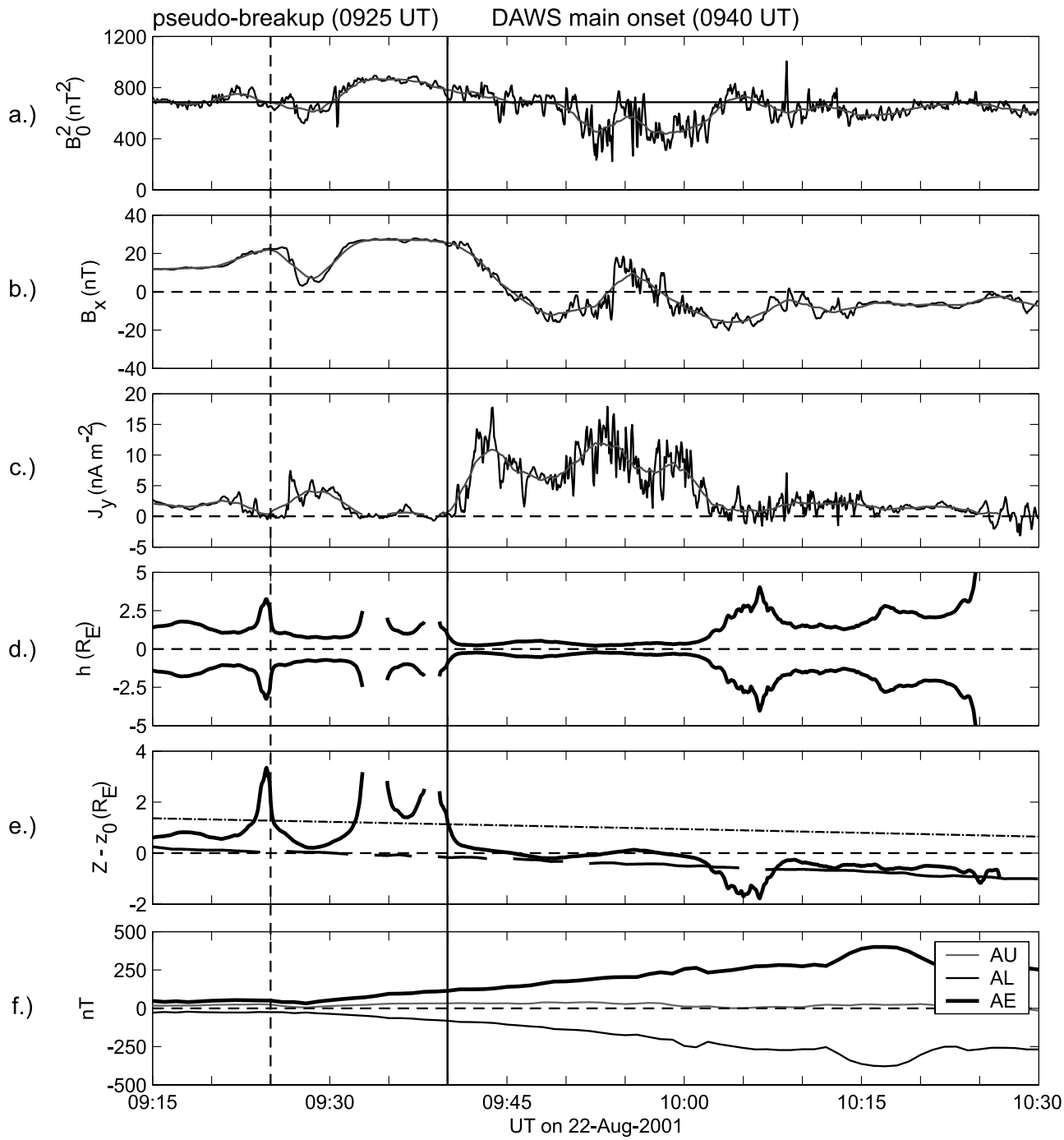

Figure 17. Temporal variation of current sheet thickness and position for the plasma sheet crossing of 22 August 2001, 0915–1030 UT. (a) B_0^2, square of the lobe magnetic field and 6-minute running average (gray). The horizontal black line shows a baseline to emphasize the growth phase increase of B_0, (b) four-spacecraft averaged B_X (black) and 6-min running average (gray), (c) J_Y and 6-min running average (gray), (d) Current sheet half-thickness h plotted with a mirror image to indicate the total thickness cross section, (e) Cluster position relative to current sheet (Z-z_0), Cluster Z position (dash-dot trace), and predicted Cluster position relative to current sheet from the *Hammond et al.* [1994] model (thin black trace), (f) Auroral indices *AU*, *AL*, and *AE*.

expected thickening following onset. We conclude from the disagreement between the parameters that we inferred for a time-varying Harris model and the predictions of the NENL model that either the time-varying Harris description is invalid for this event, substorms need not evolve as they do in the NENL model, or that delays in propagation between the premidnight and postmidnight magnetotail (see location of Cluster in Figure 5a) may complicate the phenomenological description of this event.

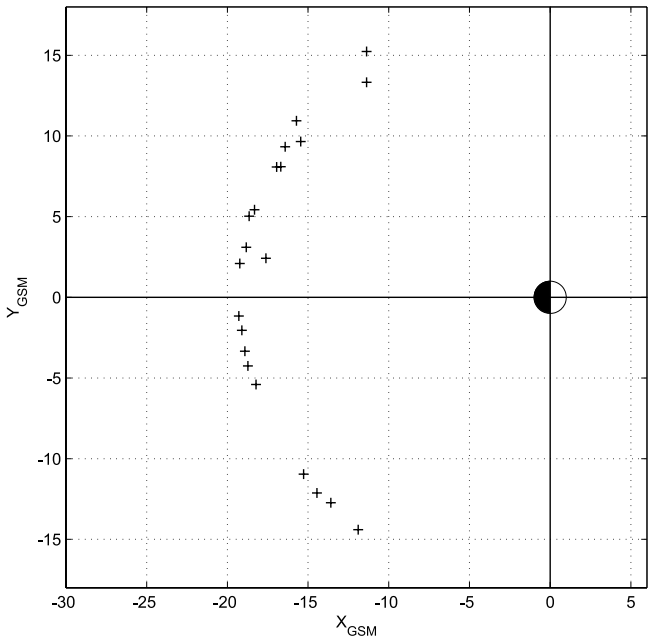

Figure 18. X-Y GSM positions of Cluster at the time of 21 local substorm onsets observed at Cluster in 2001 (13 events) and 2002 (8 events).

5.4. Superposed Epoch of Harris Current Sheet Half-Thickness

[31] The time-varying Harris model fit for current sheet thickness changes as described by the near-Earth neutral line model for two of the three substorm events presented here. Having shown that the dynamic Harris model yields plausible parameters in two of three specific cases, we investigate the current sheet behavior during a substorm using statistical methods.

[32] For plasma sheet crossings in 2001, substorm onsets were identified using the technique of *Hsu and McPherron* [1996, 1998]. The technique first identifies onsets as rapid decreases in the *AL* index greater than 100 nT that persist for at least 30 min. The north-south component of ground magnetometer data from the MEASURE array [*Moldwin and Berube*, 2004] at 1 s resolution were then bandpass filtered in the *Pi*2 frequency window (40–150 s). *Pi*2 pulsations of duration 10 min or greater observed at three or more MEASURE stations were defined as onsets. The onsets identified in the *AL* index and the onsets identified with *Pi*2 pulsations were then cross-referenced and a final substorm onset was identified as any pairing of *AL* and *Pi*2 onsets within ±20 min of each other. The *Pi*2 onset time was recorded as the substorm onset. The *Hsu and McPherron* [1996, 1998] technique identified 673 onsets in the *AL* index between 1 July and 30 November 2001, 443 of which had an associated *Pi*2 pulsation onset. Of the 443 onsets, Cluster was located in the plasma sheet (defined as $\beta > 0.1$) for 53. Substorm onsets in 2002 had to be identified in a different manner because digital *AL* index data were not available. First, plots of the north-south component of the ground magnetic field at stations of the CANOPUS, IMAGE, and 210 Magnetic Meridian were inspected for isolated substorm onsets depending on which ground stations were located in the midnight sector. Identified onset times were then compared with time intervals when Cluster was located in the plasma sheet in 2002. Signatures of the identified substorms in 2001 and 2002 were then sought in the Cluster FGM and CIS/CODIF measurements. Ion flows $\geq$200 km s^{-1} in GSM V_X at one or more Cluster spacecraft and increases of GSM $B_Z \geq 5$ nT above background (dipolarizations) within ±15 min of a particular onset were recorded as a local substorm onset at Cluster. Of the 53 *AL*/*Pi*2 onsets for which Cluster was nominally located in the plasma sheet in 2001, 13 were unambiguously identified as local onsets at Cluster. An additional eight local substorm onsets were identified in 2002.

[33] Figure 18 shows the X-Y GSM positions of Cluster at the times of the local onsets that we identified. Onsets were observed at all local times across the magnetotail and on approximately one-third of all tail orbits. For each substorm event we have taken 6-min running averages shifted by one time step (4 s for B_Z and J_Y, 8 s for B_0 and h) to reduce high-frequency fluctuations and used the averaged data to extract parameters for a Harris neutral sheet. Figure 19 shows the superposed epoch analysis of the 21 onsets for the pressure balance lobe magnetic field B_0, local $B_Z/|B|$, current density J_Y, half-thickness h, and current density multiplied with the full current sheet thickness ($2hJ_Y$) for 60 min before and 90 min after onset time (defined as epoch 0). The thick black traces indicate medians while the traces above and below the medians indicate the upper and lower quartiles, respectively. The median value of the lobe magnetic field B_0 (Figure 19a) remained relatively constant at ~28 nT in the hour preceding onset. At onset, the lobe field decreased to ~26 nT. The lobe magnetic field decreased further to ~24 nT 15 min after onset and changed little in the hour following. The overall change in lobe magnetic field was ~4 nT before and after onset, corresponding to a ~25% decrease in lobe magnetic pressure. *Caan et al.* [1978], using OGO-5, found a comparable change in lobe magnetic pressure near midnight local time in the hour before substorm onset, not including the contribution of particle pressure. *McPherron and Hsu* [2002] found increases in median lobe magnetic field of 20–30% in the hour prior to onset for substorm events observed in the tail with ISEE 2. The lack of increasing median lobe magnetic pressure during the growth phase may be the result of the large variation in local time of our substorm events. The upper quartile is relatively flat in the hour before onset, fluctuating between 32 and 34 nT. After onset, the upper quartile decreases to ~30 nT for the remainder of the epoch time. The lower quartile increases from ~23 nT to ~25 nT in the hour prior to onset and then decreases to ~17 nT 20 min after onset. The median $B_Z/|B|$ (Figure 19b) decreases from 0.25 to ~0 in the hour before onset, indicating that the magnetic field is becoming more tail-like. At onset $B_Z/|B|$ steadily increases to ~0.5 60 min after onset, reflecting dipolarization of the magnetic field during the substorm expansion phase [*Baumjohann et al.*, 1992, 1999]. The upper and lower quartiles show the same overall trend. The median cross-tail current density J_Y (Figure 19c) is ~1 nA m^{-2} 60 min prior to onset and increases steadily to ~2.5 nA m^{-2} at onset. The median current density peaks just after onset at ~3 nA m^{-2} before decreasing to ~0.5 nA m^{-2} 30 min after onset. The upper

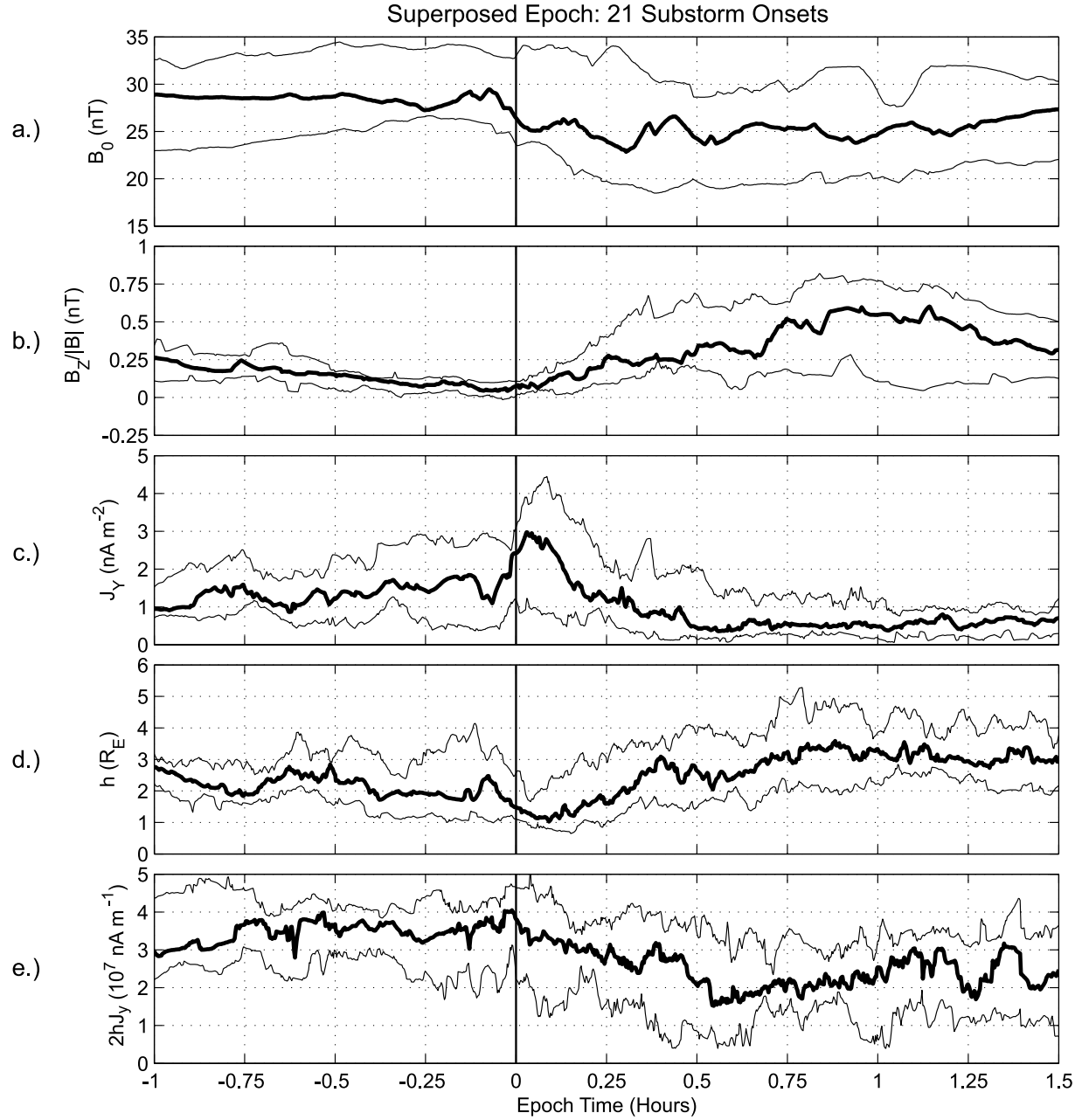

Figure 19. Superposed epoch analysis for 21 local substorm onsets identified at Cluster in 2001 and 2002. The time range covered is 45 min before and 90 min after onset. The thick black trace is the median while the upper and lower thin traces are the upper and lower quartiles, respectively. (a) Lobe magnetic field B_0, (b) $B_Z/|B|$, (c) current density J_Y, (d) Harris current sheet half-thickness h, (e) Product of current density and current sheet full thickness ($2hJ_Y$).

and lower quartiles show the same trend. Increasing current density during the growth phase is consistent with the loading of magnetic flux into the magnetotail. Higher current density is needed to produce the larger lobe magnetic field during the growth phase. Decreasing current density following onset is consistent with the removal of magnetic flux from the tail and a thicker plasma sheet. The median time-varying Harris half-thickness parameter (Figure 19d) fluctuates around 1.8–2.6 R_E between 60 and 30 min before onset. The thickness then decreases to $\sim$1 R_E just after onset and steadily increases to $\sim$3 R_E 45 min after onset. The current density multiplied with full current sheet thickness ($2hJ_Y$, Figure 19e) gives an idea of whether or not increases (decreases) in current sheet thickness are compensated by decreases (increases) in current density such that the product of the two is constant. During the growth phase, it would be natural for the current density to increase as the current sheet becomes thinner. During the expansion and recovery phases we expect the current density to decrease as the current sheet becomes thicker. The median value of $2hJ_Y$ increases from $\sim 3 \times 10^7$ nA m^{-1} to $\sim 4 \times 10^7$ nA m^{-2} in the 60 min before substorm onset. The total current then steadily decreases to $\sim$2 nA m^{-1} by 30 min after onset. The overall change in $2hJ_Y$ before and

after onset is $\sim 10^7$ nA m^{-2}, a $\sim$30% change. The upper and lower quartiles generally reproduce the median trend.

6. Discussion

[34] In this study we have implemented a time-varying Harris current sheet model fit that takes advantage of the unique Cluster vector current density dataset. Recognizing that a typical Cluster plasma sheet crossing time series might be deconstructed into a time series of Harris current sheet model fit parameters, we have evaluated the time-varying half-thickness and central (N-S) position. Our current sheet thickness parameter results are generally consistent with results from previous studies based on local magnetic field measurements [*McComas et al.*, 1986; *Sanny et al.*, 1994; *Zhou et al.*, 1997; *Asano et al.*, 2004]. *Sanny et al.* [1994] found a minimum current sheet thickness of $\sim$500 km for a case study substorm onset. *Zhou et al.* [1997] found a minimum thickness of $\sim$0.5 R_E for a case study substorm onset. As in these studies, we identified current sheets less than an R_E thick in the Cluster data. For three case study events presented here, we found minimum current sheet thicknesses of $\sim$1000 km and $\sim$1 R_E. Thin current sheets have received a great deal of attention in recent years because they are believed to be important in the development of substorm onset in the magnetotail. In particular, the near-Earth neutral line is believed to form at a thin current sheet somewhere between 20 and 30 R_E downtail [e.g., *Nakamura et al.*, 1994; *Nagai et al.*, 1998]. Some events in our Cluster data set reveal thin current sheets and the near-Earth neutral line itself at or inside of $\sim$20 R_E downtail. The case study events presented here have strong earthward and tailward flows in addition to clear Hall current B_Y perturbations that place the neutral line within $X \sim -19$ R_E. Because Cluster dwells near the neutral sheet of the magnetotail for long intervals near apogee, it is better situated than many previous spacecraft (ISEE 1 and 2 and AMPTE/IRM, for example) to observe signatures associated with such very close locations of the neutral line. Whereas the probability that a neutral line forms inside of 20 R_E downtail may be lower than at 20–30 R_E, the Cluster data show that it is not unusual for the near-Earth neutral line to be present at distances closer than generally suggested. Our ideas of the probability of observing the neutral line close to Earth are challenged as a consequence of these Cluster observations. The thin current sheets discussed in this paper are also relevant to studies of bifurcated current sheets, which will be explored in a future publication.

[35] The superposed epoch analysis of lobe magnetic field B_0, B_Z, current sheet thickness, and total current produced results generally consistent with the near-Earth neutral line model for substorms. However, the median lobe magnetic field did not clearly increase during the growth phase, as predicted by the NENL model [*McPherron et al.*, 1973; *Russell and McPherron*, 1973; *McPherron*, 1991]. However, the lower quartile lobe field did show a growth phase increase. It is possible that the growth phase increase of lobe magnetic flux is more pronounced when the preexisting lobe magnetic field magnitude is lower or that the full sequence of changes postulated in the NENL model occurs only for isolated substorms. The $B_Z/|B|$ ratio clearly showed the decrease of B_Z expected during the growth phase as the magnetic field becomes more tail-like. The steady increase of B_Z after onset reflects the dipolarization of the magnetic field. However, one of our definitions for substorm onset at Cluster was an increase in B_Z, so this result is not surprising. The cross-tail current density J_Y showed the gradual increase in current density expected during the growth phase as the plasma sheet thins followed by a steady decrease during the recovery phase as the plasma sheet thickens. Our current sheet half-thickness parameter gradually decreased during the growth phase, reached a minimum near onset, and then steadily increased during the recovery phase. The total current slightly increased prior to onset but clearly decreased after onset, as expected from the NENL model.

[36] An interesting question concerning the cross-tail current, J_Y, is how significant a contribution the spatial gradient of B_Z with X makes to the overall current. Cluster provides the nine spatial gradients of the magnetic field necessary to calculate the curl and divergence of **B**. The Y-component of $\nabla \times \mathbf{B}$ is

$$J_Y = \mu_0(\nabla \times B)_Y = \mu_0\left(\frac{\partial B_X}{\partial Z} - \frac{\partial B_Z}{\partial X}\right) \quad (6)$$

In simplified pictures of the magnetotail the magnetic field is almost entirely in the solar or antisolar direction and $\partial B_Z/\partial X$ is negligible. However, at the $\sim$20 R_E apogee distance of Cluster in the magnetotail magnetic field lines may be sensitive to the stretched dipolar field lines of the inner magnetosphere. There are often significant changes in B_Z in this region that may generate cross-tail current. Dynamic changes in the magnetotail resulting from substorms can also generate large variations in B_Z that have significant gradients in X. We expect large changes in B_Z during the expansion and recovery phases of a substorm [e.g., *Baumjohann et al.*, 1991, 1992]. The structure of the magnetic field near a reconnection X-line also exhibits rapid changes in B_Z. To examine the relative contribution of $\partial B_Z/\partial X$ to the cross-tail current density during substorms, we have constructed a superposed epoch plot of the ratio of $|\partial B_Z/\partial X|$ to $|\partial B_X/\partial Z|$ at 4-s resolution for the 21 local substorm onsets identified at Cluster for this study. Figure 20 shows the median and quartiles of the ratio for ±60 min around local substorm onset in the same format as Figure 19. The median ratio before onset shows that $\partial B_Z/\partial X$ is no more than 5–10% of $\partial B_X/\partial Z$ prior to onset, which is expected because B_Z becomes small over large portions of the plasma sheet during the growth phase. However, the upper quartile shows that $\partial B_Z/\partial X$ can approach 50% of $\partial B_X/\partial Z$ at times. In the 60 min after onset, the median ratio fluctuates considerably between 0.2 and 0.5 and the upper quartile often exceeds 1. This likely indicates the dipolarization of the magnetic field during the substorm expansion phase. As the local B_Z increases and the plasma sheet thickens earthward of the neutral line, $\partial B_Z/\partial X$ can contribute substantially to J_Y and to canceling the part of $\partial B_X/\partial Z$ that arises from the internal multipoles. This superposed epoch analysis reveals that $\partial B_Z/\partial X$ can sometimes make a nonnegligible contribution to the total cross-tail current density, particularly during disturbed times. Despite this, previous studies that calculated current sheet thickness with ISEE 1 and 2 are acceptable because

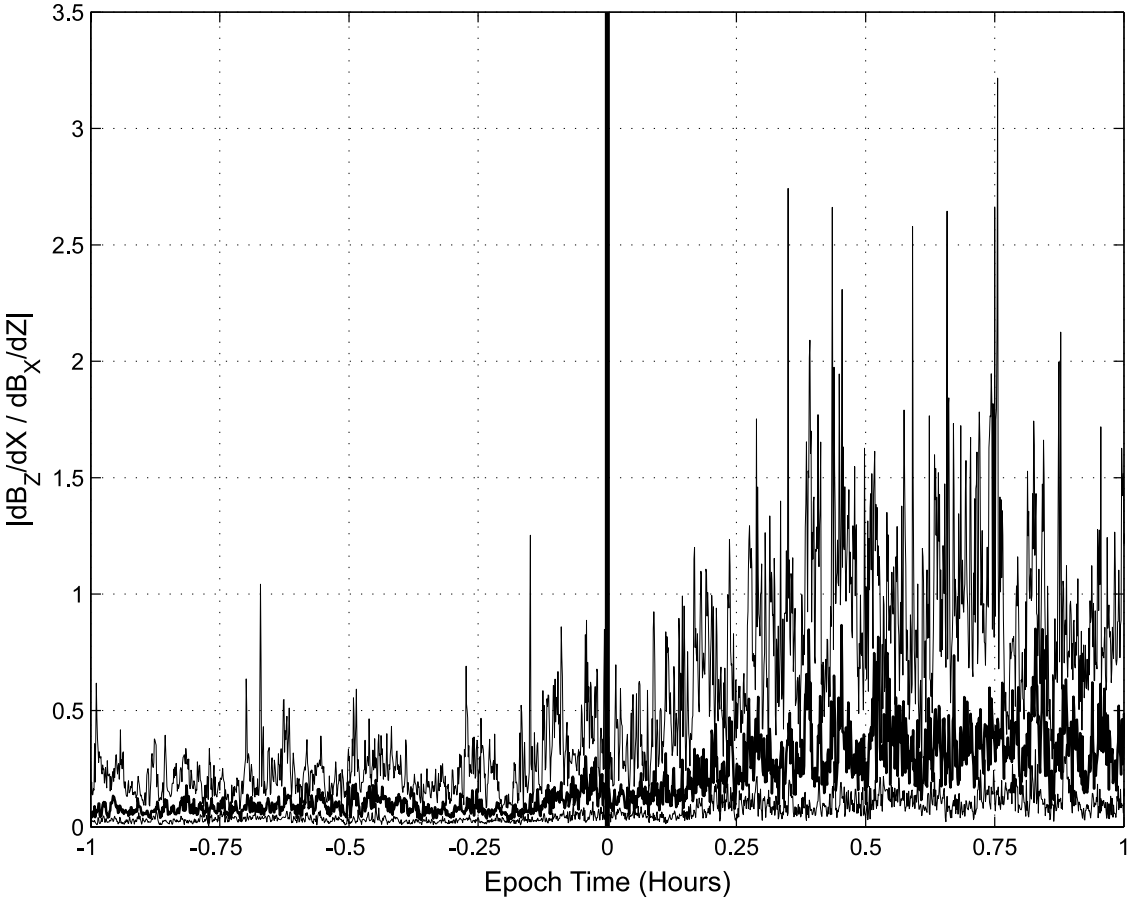

Figure 20. Superposed epoch analysis of $dB_Z/dX/dB_X/dZ$ for 21 substorm onsets identified at Cluster in 2001 and 2002. The time range covered is 60 min before and after substorm onset at Cluster.

most of the time $\partial B_Z/\partial X \ll \partial B_X/\partial Z$. These studies were hampered by brief conjunctions and large spacecraft separations but their results offer a reasonable approximation to the results provided by Cluster.

[37] The demonstration that $\partial B_Z/\partial X$ can at times contribute significantly to J_Y raises the question of whether or not our pressure balance determination of lobe magnetic field is reliable. In calculating the lobe field, we assume the tension component of $\mathbf{J} \times \mathbf{B}$ ($\mathbf{B} \times \nabla\mathbf{B}/\mu_0$) is negligible. However, at times when $\partial B_Z/\partial X$ is nonnegligible, the tension component contributes to pressure balance. We calculated the contribution of the tension component to pressure balance at times when $\partial B_Z/\partial X$ is nonnegligible and found that in some instances the tension contribution should not be ignored. However, in the scope of all of our events, these times are few. Furthermore, our methodology is primarily concerned with pressure balance in the z direction. When the tension component is most likely to be relevant (in the current sheet), the tension force is directed predominantly in the x direction. As a result, the tension should have little impact on pressure balance in the z direction. We therefore believe that our lobe magnetic field and subsequent calculation of current sheet thickness are generally reliable.

7. Summary and Conclusions

[38] We have implemented an inversion of the Harris current sheet model that takes advantage of the new Cluster vector current density dataset. Our results for three case study substorm events and a superposed epoch analysis showed that thin current sheets can be found during the substorm growth phase at the 20 R_E downtail distance of Cluster and that plasma sheet thinning and thickening often follow the sequence described by the NENL model. Multipoint magnetometer and particle observations reveal that the neutral line can form earthward of ~19 R_E downtail and that $\partial B_Z/\partial X$ can make a significant contribution to the cross-tail current density around substorm onset.

[39] **Acknowledgments.** This work was supported by the University of California Institute of Geophysics and Planetary Physics Los Alamos National Laboratory under grant 1113-R and NASA under grant NAG 5-12131. We wish to thank the Magnetospheric Physics Group at UCLA for its evaluation of this work, C. Mouikis for providing CIS/CODIF data, H. Schwarzl for careful calibrations of the Cluster magnetometer data, and T.-S. Hsu for providing the *Pi2/AL* substorm onset database for 2001. The ACE solar wind data were acquired from the ACE Science Center online database. The ACE MAG data were provided by the Bartol Research Institute and Goddard Space Flight Center. The ACE SWEPAM data were provided by the Los Alamos National Laboratory and Sandia National Laboratory. We thank the Finnish Meteorological Institute for IMAGE magnetometer array data. The CANOPUS instrument array, constructed, maintained, and operated by the Canadian Space Agency, provided the CANOPUS magnetometer data used in this study. We thank K. Yumoto and K. Shiokawa for 210 Magnetic Meridian data. The 210 Magnetic Meridian database constructed at the Solar-Terrestrial Environment Laboratory, Nagoya University. Auroral indices were acquired from the World Data Center for Geomagnetism, Kyoto. We thank K. Stasiewicz, M. Khotyaintsev, and Y. Khotyaintsev and the Orbital Visualization Team at the Swedish

Institute of Space Physics for the OVT application http://ovt.irfu.se). UCLA Institute of Geophysics and Planetary Physics publication 6197.

[40] Lou-Chuang Lee thanks Goetz Paschmann and another reviewer for their assistance in evaluating this paper.

References

Asano, Y., T. Mukai, M. Hoshino, Y. Saito, H. Hayakawa, and T. Nagai (2004), Current sheet structure around the near-Earth neutral line observed by Geotail, *J. Geophys. Res.*, *109*, A02212, doi:10.1029/2003JA010114.

Balogh, A., et al. (2001), The Cluster magnetic field investigation: Overview of in-flight performance and initial results, *Ann. Geophys.*, *19*, 1207.

Baumjohann, W. (1993), The Near-Earth plasma sheet: An AMPTE/IRM perspective, *Space Sci. Rev.*, *64*, 141.

Baumjohann, W., G. Paschmann, and H. Luhr (1990), Pressure balance between lobe and plasma sheet, *Geophys. Res. Lett.*, *17*, 45.

Baumjohann, W., G. Paschmann, T. Nagai, and H. Luhr (1991), Superposed epoch analysis of the substorm plasma sheet, *J. Geophys. Res.*, *96*, 11,605.

Baumjohann, W., G. Paschmann, and T. Nagai (1992), Thinning and expansion of the substorm plasma sheet, *J. Geophys. Res.*, *97*, 17,173.

Baumjohann, W., M. Hesse, S. Kokubun, T. Mukai, T. Nagai, and A. A. Petrukovich (1999), Substorm dipolarization and recovery, *J. Geophys. Res.*, *104*, 24,995.

Caan, M. N., R. L. McPherron, and C. T. Russell (1978), The statistical magnetic signature of magnetospheric substorms, *Planet. Space Sci.*, *26*, 269.

Cowley, S. W. H., and W. J. Hughes (1983), Observation of an IMF sector effect in the Y magnetic field component at geostationary orbit, *Planet. Space Sci.*, *31*, 73.

Dandouras, J. (1988), On the average shape and position of the geomagnetic neutral sheet and its influence on plasma sheet statistical studies, *J. Geophys. Res.*, *93*, 7345.

Dennis, J. E., Jr. (1977), Nonlinear least-squares, in *State of the Art in Numerical Analysis*, edited by D. Jacobs, pp. 269–312, Elsevier, New York.

Fairfield, D. H. (1980), A statistical determination of the shape and position of the geomagnetic neutral sheet, *J. Geophys. Res.*, *85*, 775.

Fairfield, D. H., R. P. Lepping, E. W. Hones Jr., S. J. Bame, and J. R. Asbridge (1981), Simultaneous measurements of magnetotail dynamics by IMP spacecraft, *J. Geophys. Res.*, *86*, 1396.

Hammond, C. M., M. G. Kivelson, and R. J. Walker (1994), Imaging the effect of dipole tilt on magnetotail boundaries, *J. Geophys. Res.*, *99*, 6079.

Harris, E. G. (1962), On a plasma sheet separating regions of oppositely directed magnetic field, *Nuovo Cimento*, *23*, 115.

Holzworth, R. H., and C.-I. Meng (1975), Mathematical representation of the auroral oval, *Geophys. Res. Lett.*, *2*, 377.

Hsu, T.-S., and R. L. McPherron (1996), Occurrence frequency of substorm field and plasma signatures observed near-earth by ISEE-1/2, in *Proceedings of the Third International Conference on Substorms (ICS-3)*, edited by E. J. Rolfe and B. Kaldeich, p. 333, Eur. Space Agency, Versailles, France.

Hsu, T.-S., and R. L. McPherron (1998), The main onset of a magnetospheric substorm, in *Proceedings of the Fourth International Conference on Substorms (ICS-4)*, edited by S. Kokubun and Y. Kamide, p. 79, Terra Sci., Tokyo.

Khurana, K. K., E. L. Kepko, M. G. Kivelson, and R. C. Elphic (1996), Accurate determination of magnetic field gradients from four-point vector measurements 2: Use of natural constraints on vector data obtained from four spinning spacecraft, *IEEE Trans. Magn.*, *32*, 5193.

Li, L., and R. L. Xu (2000), A neutral sheet surface observed on ISEE-2, IMP-8, AMPTE/IRM, and INTERBALL satellites, *Geophys. Res. Lett.*, *27*, 855.

Lühr, H., A. Aylward, S. C. Buchert, A. Pajunpää, K. Pajunpää, T. Holmboe, and S. M. Zalewski (1998), Westward moving dynamic substorm features observed with the IMAGE magnetometer network and other ground-based instruments, *Ann. Geophys.*, *16*, 425.

Lui, A. T. Y. (1993), Inferring global characteristics of current sheet from local measurements, *J. Geophys. Res.*, *98*, 13,423.

Matsumoto, Y., T. Mukai, Y. Saito, S. Kokubun, and M. Hoshino (2001), On the pressure balance in the distant magnetotail, *J. Geophys. Res.*, *106*, 25,905.

McComas, D. J., C. T. Russell, R. C. Elphic, and S. J. Bame (1986), The near-earth cross-tail current sheet: Detailed ISEE 1 and 2 case studies, *J. Geophys. Res.*, *91*, 4287.

McPherron, R. L. (1991), Physical processes producing magnetospheric substorms and magnetic storms, in *Geomagnetism*, vol. 4, edited by J. Jacobs, p. 593, Elsevier, New York.

McPherron, R. L., and T.-S. Hsu (2002), A comparison of substorms occurring during magnetic storms with those occurring during quiet times, *J. Geophys. Res.*, *107*(A9), 1259, doi:10.1029/2001JA002008.

McPherron, R. L., C. T. Russell, and M. Aubry (1973), Satellite studies of magnetospheric substorms on August 15, 1978: 9, Phenomenological model for substorms, *J. Geophys. Res.*, *78*, 3131.

McPherron, R. L., A. Nishida, and C. T. Russell (1987), Is near-Earth current sheet thinning the cause of auroral substorm onset?, in *Quantitative Modeling of the Magnetosphere-Ionosphere Coupling Processes*, edited by Y. Kamide and R. A. Wolf, p. 252, Kyoto Sangyo Univ., Kyoto, Japan.

Moldwin, M. B., and D. Berube (2004), ULF resonance monitoring of diurnal plasmaspheric refilling: Results from the MEASURE magnetometer array, *Eos Trans. AGU*, *85*(17), Jt. Assem. Suppl., Abstract SM31A-09.

Nagai, T., M. Fujimoto, Y. Saito, S. Machida, T. Terasawa, R. Nakamura, T. Yamamoto, T. Mukai, A. Nishida, and S. Kokubun (1998), Structure and dynamics of magnetic reconnection for substorm onsets with Geotail observations, *J. Geophys. Res.*, *103*, 4419.

Nagai, T., I. Shinohara, M. Fujimoto, M. Hoshino, Y. Saito, S. Machida, and T. Mukai (2001), Geotail observations of the Hall current system: Evidence of magnetic reconnection in the magnetotail, *J. Geophys. Res.*, *106*, 25,929.

Nakamura, R., D. N. Baker, D. H. Fairfield, D. G. Mitchell, R. L. McPherron, and E. W. Hones Jr. (1994), Plasma flow and magnetic field characteristics near the midtail neutral sheet, *J. Geophys. Res.*, *99*, 23,591.

Nakamura, R., et al. (2002), Fast flow during current sheet thinning, *Geophys. Res. Lett.*, *29*(23), 2140, doi:10.1029/2002GL016200.

Ness, N. F. (1965), The earth's magnetic tail, *J. Geophys. Res.*, *70*, 2989.

Rème, H., et al. (2001), First multispacecraft ion measurements in and near the Earth's magnetosphere with the identical Cluster Ion Spectrometry (CIS) experiment, *Ann. Geophys.*, *19*, 1303.

Rich, F. J., V. M. Vasyliunas, and R. A. Wolf (1972), On the balance of stresses in the plasma sheet, *J. Geophys. Res.*, *77*, 4670.

Runov, A., R. Nakamura, W. Baumjohann, T. L. Zhang, M. Volwerk, H.-U. Eichelberger, and A. Balogh (2003), Cluster observation of a bifurcated current sheet, *Geophys. Res. Lett.*, *30*(2), 1036, doi:10.1029/2002GL016136.

Russell, C. T., and K. I. Brody (1967), Some remarks on the position and shape of the neutral sheet, *J. Geophys. Res.*, *72*, 6104.

Russell, C. T., and R. L. McPherron (1973), The magnetotail and substorms, *Space Sci. Rev.*, *11*, 111.

Sanny, J., R. L. McPherron, C. T. Russell, D. N. Baker, T. I. Pulkkinen, and A. Nishida (1994), Growth-phase thinning of the near-Earth current sheet during the CDAW 6 substorm, *J. Geophys. Res.*, *99*, 5805.

Sergeev, V., et al. (2003), Current sheet flapping motion and structure observed by Cluster, *Geophys. Res. Lett.*, *30*(6), 1327, doi:10.1029/2002GL016500.

Shen, C., X. Li, M. Dunlop, Z. X. Liu, A. Balogh, D. N. Baker, M. Hapgood, and X. Wang (2003), Analyses on the geometrical structure of magnetic field in the current sheet based on cluster measurements, *J. Geophys. Res.*, *108*(A5), 1168, doi:10.1029/2002JA009612.

Sonnerup, B. U. Ö. (1979), Magnetic field reconnection, in *Solar System Plasma Physics*, vol. III, edited by L. T. Lanzerotti, C. F. Kennel, and E. N. Parker, pp. 45–108, North-Holland, New York.

Tsyganenko, N. A. (1995), Modeling the Earth's magnetospheric magnetic field confined within a realistic magnetopause, *J. Geophys. Res.*, *100*, 5599.

Weygand, J. M., et al. (2005), Plasma sheet turbulence observed by Cluster II, *J. Geophys. Res.*, *110*, A01205, doi:10.1029/2004JA010581.

Zhou, X.-Y., C. T. Russell, J. T. Gosling, and D. G. Mitchell (1997), Three spacecraft observations of the geomagnetic tail during moderately disturbed conditions: Structure and evolution of the current sheet, *J. Geophys. Res.*, *102*, 14,415.

A. Balogh, Space and Atmospheric Physics Group, The Blackett Laboratory, Imperial College, Prince Consort Road, London, SW7 2 BZ, UK.

K. K. Khurana, M. G. Kivelson, R. L. McPherron, S. M. Thompson, and J. M. Weygand, Institute of Geophysics and Planetary Physics, University of California, Los Angeles, 405 Hilgard Avenue, Los Angeles, CA 90095-1567, USA. (mkivelson@igpp.ucla.edu; sthompson@igpp.ucla.edu)

L. M. Kistler, Space Science Center, Science and Engineering Research Center, University of New Hampshire, Durham, NH 03824, USA.

H. Réme, Centre d'Etude Spatiale des Rayonnements/Centre National de Recherche Scientifique, 9 Avenue du Colonel Roche, B. P. 4346, F-31028 Toulouse Cedex 4, France.

Figure 8. Cluster FGM and CIS/CODIF observations on 13 September 2001 1700–1900 UT in GSM coordinates. FGM data from all four Cluster spacecraft are plotted while CIS/CODIF data are plotted for Cluster 1 and 4. The vertical black line indicates the substorm onset at IMAGE. (a) B_X, (b) B_Y, (c) B_Z, (d) B, (e) V_X, (f) V_Y, (g) V_Z, (h) proton number density n, (i) neutral line schematic for the geometry of the magnetotail.

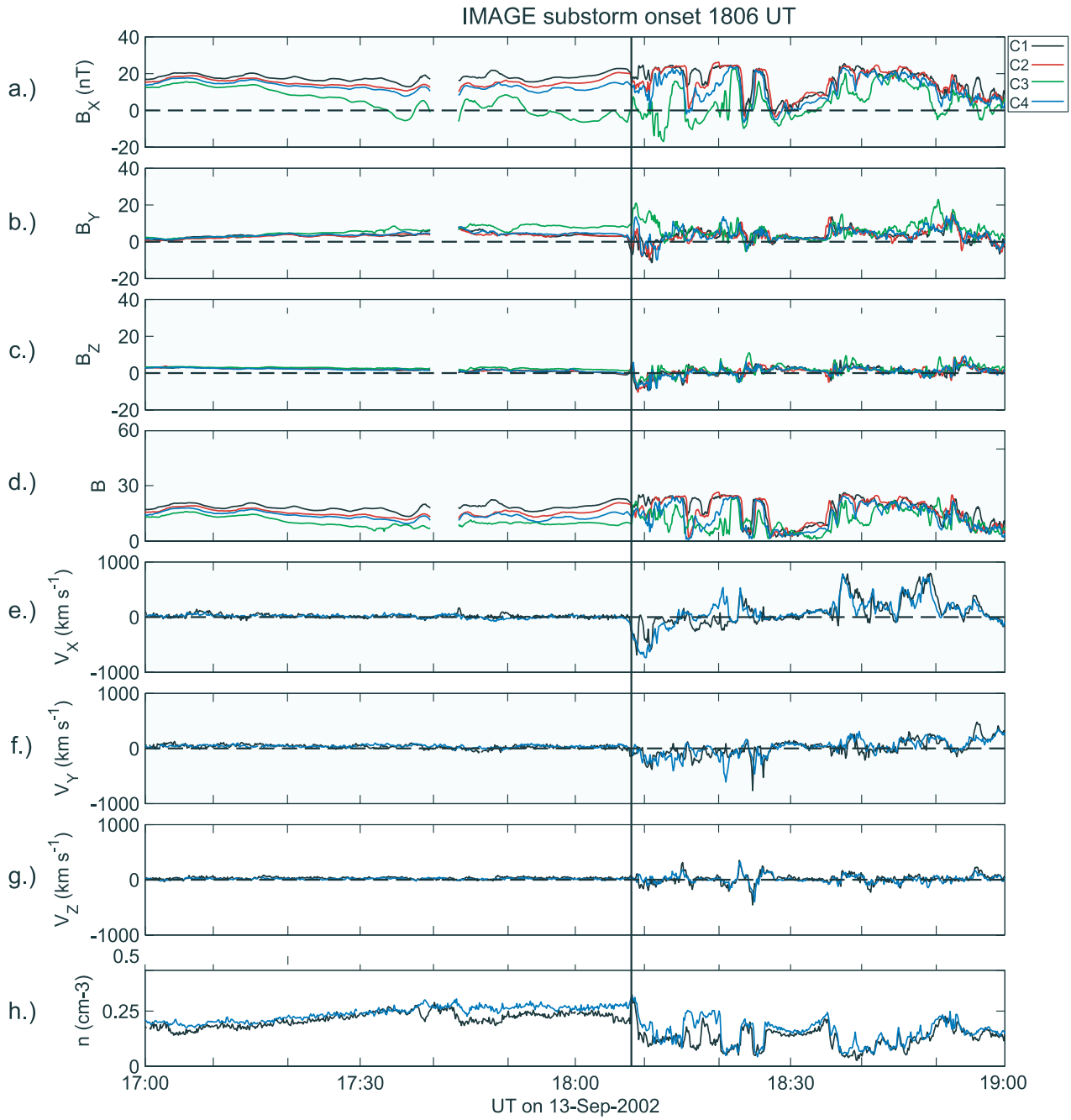
IMAGE substorm onset 1806 UT
a.)
b.)
c.)
d.)
e.)
f.)
g.)
h.)
i.)
C1
C2
C3
C4
B_X (nT)
B_Y
B_Z
B
V_X (km s^{-1})
V_Y (km s^{-1})
V_Z (km s^{-1})
n (cm-3)
17:00
17:30
18:00
18:30
19:00
UT on 13-Sep-2002
inflow
X-line
outflow
Hall current
Hall current
B_Y
B_Y
Z
X
Y

Figure 8

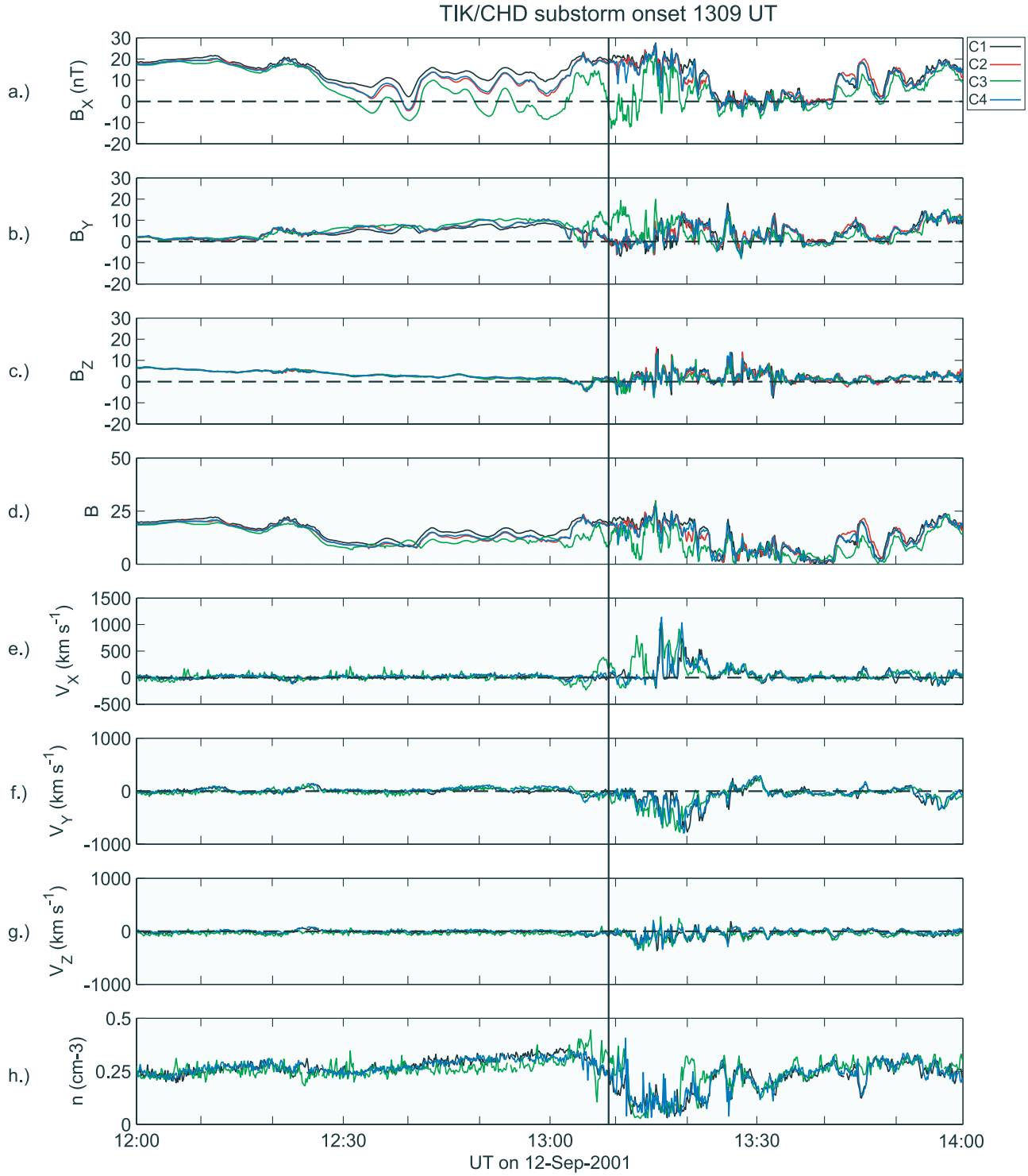

Figure 12. Cluster FGM and CIS/CODIF observations on 12 September 2001, 1200–1400 UT in GSM coordinates. FGM data from all four Cluster spacecraft are plotted while CIS/CODIF data are plotted for Cluster 1, 3, and 4. The vertical black line indicates the substorm onset at TIK and CHD. (a) B_X, (b) B_Y, (c) B_Z, (d) B, (e) V_X, (f) V_Y, (g) V_Z, (h) proton number density n.

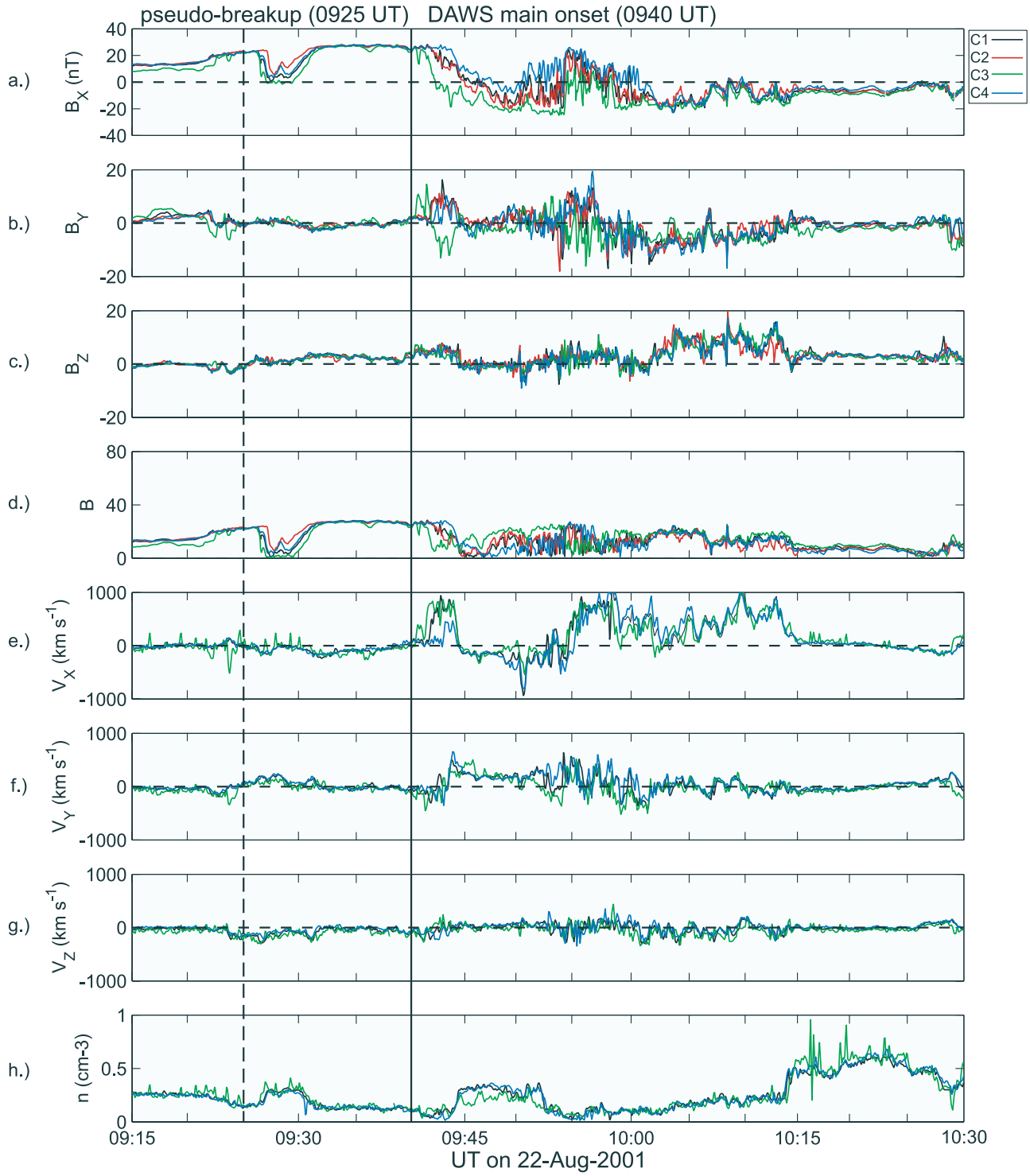

Figure 16. Cluster FGM and CIS/CODIF observations on 22 August 2001, 0915–1030 UT in GSM coordinates. FGM data from all four Cluster spacecraft are plotted while CIS/CODIF data are plotted for Cluster 1, 3, and 4. The vertical black line indicates the main onset at DAWS. The vertical dashed line indicates a likely pseudo-breakup. (a) B_X, (b) B_Y, (c) B_Z, (d) B, (e) V_X, (f) V_Y, (g) V_Z, (h) proton number density n.